HIGH QUALITY CODING AND RECONSTRUCTION FOR TRANSMISSION OF SINGLE VIDEO IMAGES

by

GERRIT BARNARD

Submitted in partial fulfilment for the requirements

of the degree

MASTER OF ELECTRONIC ENGINEERING

in the

Faculty of Engineering

University of Pretoria

November 1990

Hoë kwaliteit rekonstruksie en kodering vir transmissie van enkel videobeelde

deur

Gerrit Barnard

voorgelê ter vervulling van 'n deel van die vereiste

vir die graad

MIng

in die Fakulteit Ingenieurswese

Universiteit van Pretoria

November 1990

ABSTRACT

Title: High quality coding and reconstruction for transmission of single video images.

Candidate: Gerrit Barnard

Promoter: Prof. J.J.D. van Schalkwyk

Department: Faculty of Electronical and Computer Engineering

Degree: MEng

High quality coding of images for transmission requires complete exploitation of all the redundancies present in most images. Redundancy is present in both the statistical and psychovisual properties of images. A detailed analysis was made of the origins of perceivable distortion in images. In the section addressing coefficient quantisation, it has been found that the use of uniform quantisation followed by source coding gives better results than can be achieved with the Lloyd-Max type quantisers. An algorithm has been presented that minimises this distortion for a given coding rate with the introduction of minimal artifacts. A major contribution towards the reduction of the visible distortion was achieved by using the lapped orthogonal transform together with adaptive quantisation. This reduced the visual perception of the so called "block effect". Other aspects investigated included the use of the human visual system to determine the importance of the coefficients during quantisation, and the effect that channel errors have on some of the algorithms.

SAMEVATTING

Titel: Hoë kwaliteit rekonstruksie en kodering vir transmissie van enkel videobeelde.

Kandidaat: Gerrit Barnard

Leier: Prof J J D van Schalkwyk

Departement: Elektroniese en Rekenaaringenieurswese

Graad: MIng

Wanneer beelde gekodeer word om so hoog as moontlike kwaliteit te verkry moet die statistiese en psigovisuele oortolligheid in so 'n beeld ten volle benut word. 'n Detail studie van die oorsake van waarneembare vervorming in 'n beeld is gemaak. Uit die studie is die nodige resultate verkry om 'n algoritme voor te stel wat die waarneembare vervorming minimiseer. Daar is gevind dat die gebruik van 'n transformasie wat oor die grense van 'n blokkie strek die steurende blok-effek drasties verminder het, veral wanneer dit gekombineer is met aanpasbare kwantiseering. Verder is die oordragsfunksie van die mens se oog gebruik om tydens kwantisering te bepaal watter koëffisiente die meeste inligting dra. In die ondersoek na optimale kwantisering is daar gevind dat uniforme kwantisering gevolg deur bron-kodering beter resultate lewer as die Lloyd-Max tipe kwantiseerders. Daar is ook gekyk na die invloed wat kanaalfoute op die verkillende algoritmes het, en daar is vasgestel dat die gebruik van 'n oorvleuelende transformasie die effek van kanaalfoute verminder.

Table Of Contents

I. Introduction

Image coding has been an active area of research for many years. It is defined as the process in which the number of bits needed to represent an image is minimised subject to some quality criterion. Transform image coding has been found to be an efficient means by which to achieve this minimisation [1,2,4,7]. Thus, this thesis will not investigate image coding in general, since it is a very wide field, but a thorough investigation of all aspects regarding *transform image coding* will be given[1].

Intraframe or single image coding of video images has several applications including reconnaissance, remote sensing, and is used in interframe coding for encoding of difference images. The transmission of images over a bandwidth limited channel places constraints on the time in which the images can be transmitted. Lower average bit rates result in less data to be transmitted and consequently faster transmission rates.

Image coding techniques can be classified as either noiseless or minimum distortion. In noiseless image coding, the image is reconstructed perfectly from the coded information. The compression ratio that can be achieved, from information theory, is limited to the entropy of the image and is typically more than two bits per pel (pixel or picture element). This is not sufficient since the average bit rate

[1] For a more general discussion of image coding the reader is referred to W.K.Pratt "Digital Image Processing" John Wiley & Sons 1978.

required by most applications is less than one bit/pel. Compression ratios of this order can only be achieved at some expense in fidelity. Shannon introduced the concept of the "rate distortion function" specifically to give a mathematical framework for this kind of problem. The rate distortion function determines the minimum channel capacity required to transmit data with a specified distortion percentage subject to a suitable distortion measure.

The desired bit rates, that the algorithms will have to achieve, is between 2.0 and 0.5 bits/pel. This means that in most cases the algorithms will introduce a certain amount of distortion, and thus can be categorised under the rate distortion theory. The rate distortion function is rarely used in image coding since no representative statistical model exists for images and the definition of a suitable distortion criteria is troublesome. However, it can be used to find an absolute upper bound on the achievable performance of any image coder for a given set of images. Using the rate distortion theory, images will be generated that should give one a subjective idea of what the optimum codec will be able to achieve. These images can then be used to determine the subjective efficiency of a specific codec.

Most applications require that the reconstructed image be as close as possible to the original with little or no artifacts. This raises the question of the determination of the *quality* or *fidelity* of the image. In the rate distortion theory, the problem is one of finding a suitable distortion criteria. In most applications the user of the video

information will be a human interpreter. This places a subjective image criteria on the evaluation of the quality of a reconstructed image. In section VI the question of image fidelity is discussed briefly. The conclusion reached in that section is that a human visual weighted mean square error gives an acceptable image fidelity measure, although the mean square error itself will also be used for comparison purposes. The use of the human visual system in the image coding environment has been widely publicised [4,7]. However, it has been found that care should be taken in the application of these models since they depend on certain physical parameters, such as the viewing angle, that the user might want to adapt. The viewing angle might change considerable if the sections of the image is magnified. In general the incorporation of the model of the human visual system will increase the performance of the image coder since it provides additional information regarding the image coding system [1,2,7]. The model of the human visual system developed by Mannos and Sakrison [16] were used in the experiments.

The thesis was started with an investigation into the different types of distortion that is generated during the coding process. The origins of the distortions were categorised according to quantisation and block processing noise. Of the different sources of noise the block processing noise, generated by the independent processing of blocks, was found to generate the most subjective objectionable distortion, namely the *block-effect*. An efficient solution to this problem, using an

overlapping transform, was given by Cassereau [61]. The specific transform was called the lapped orthogonal transform (LOT). Another technique that reduces the block-effect and also improves overall coder performance is the use of a visual error criterium in the assignment of bits for quantisation. A feasible method to incorporate the visual system into transform coding was given by Eggerton [56].

The final goal of the image coding system is the transmission of the coded image over a transmission channel. Therefore the effect of channel errors had to be kept in mind in the design of the image codec's. Since channel errors are more serious when the data is represented efficiently, the addition of a controlled form of redundancy, in the form of error detection and correction schemes, is necessary [3]. The evaluation of different error coding schemes did not form part of the thesis but the effect of channel errors on the different types of data, i.e. quantisation information and coded coefficients, present in the encoded stream were investigated.

A. Thesis Structure

It was decided to divide the thesis into problem statement and problem solving sections. The thesis starts with a general background to transform image coding, which include a simplistic but relatively efficient image codec. The sources of errors in this basic transform image codec is investigated and presented. The next sections presents possible solutions to the identified errors. A diagrammatical representation of the structure of the thesis is shown in figure 1.

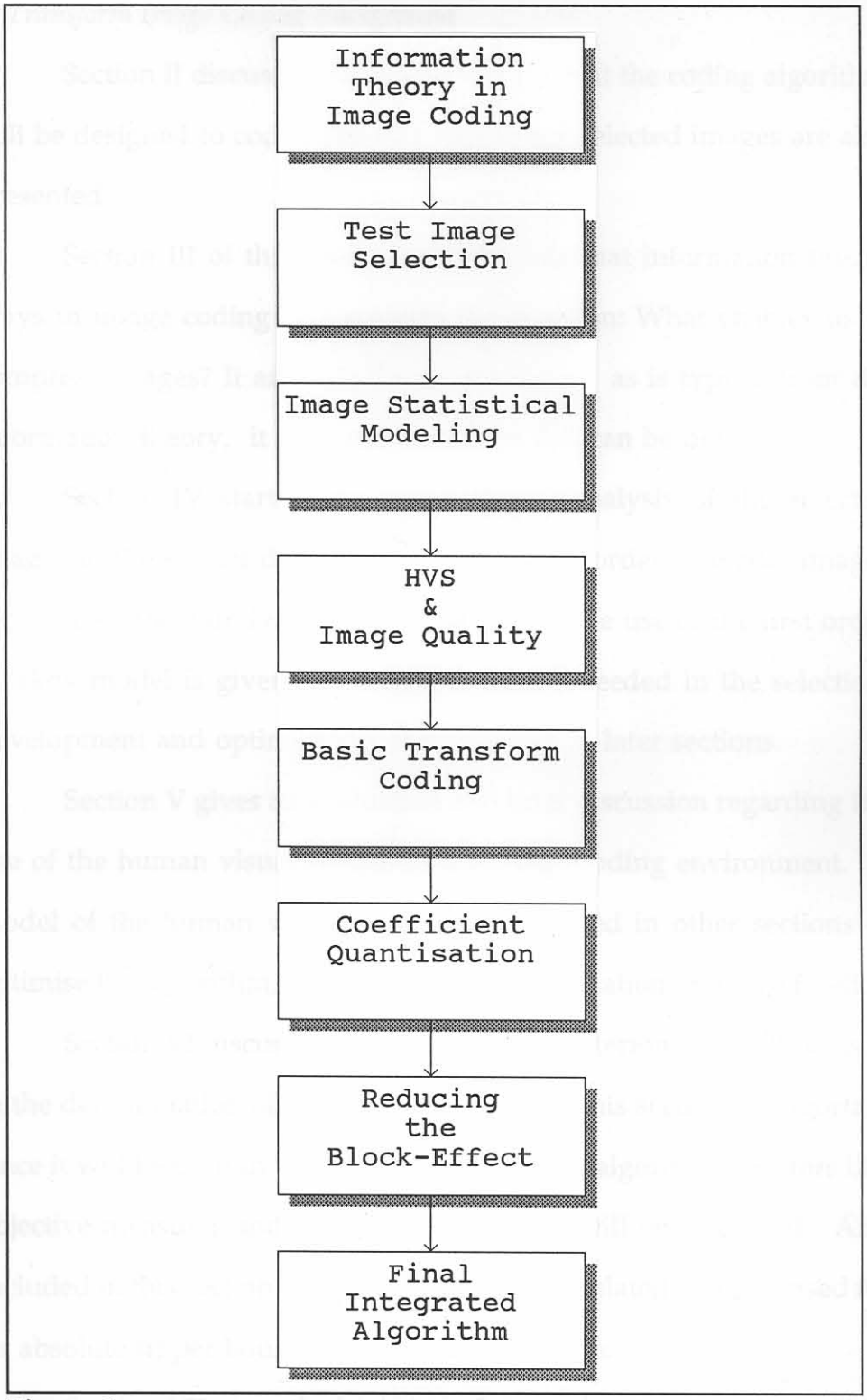

Figure 1 Diagrammatic representation of the thesis structure.

1. Transform Image Coding Background

Section II discusses the type of images that the coding algorithm will be designed to code. The originals of the selected images are also presented.

Section III of this thesis states the role that information theory plays in image coding and answers the question: What enables us to compress images? It answers the question but, as is typical from the information theory, it does not state how this can be done.

Section IV starts with the statistical analysis of the selected images in the spatial domain. This is done in order to model images for mathematical derivations. The reason for the use of the first order Markov model is given. This model will be needed in the selection, development and optimisation of transforms in later sections.

Section V gives an evaluation and brief discussion regarding the use of the human visual system in the image coding environment. A model of the human visual system will be used in other sections to optimise the algorithm, and also in the determination of image fidelity.

Section VI discusses the image quality criterion that will be used in the determination of coded image quality. This section is important since it will be used in the synthesis of the final algorithm. Factors like objective measures and subjective evaluation will be discussed. Also included in this section is the rate distortion simulated images, used for an absolute upper bound on codec performance.

Section VII gives the basic transform coder structure that will be used as a starting point. The functions of the basic structures is investigated and sources of errors is identified and discussed.

2. Codec Optimisation

The following sections are aimed at optimising the image codec, in order to minimise the observed coding-error.

Section VIII looks at improving quantisation by using statistical models, making the quantisation adaptive, and using source coding.

Section IX looks at methods for reducing the block effect at low bit rates. This includes using the human visual system model, spatially variant filtering and overlapping transforms.

Section X puts the different subsections together and evaluates the system's overall performance, including performance in the presence of channel errors.

Section XI contains the concluding remarks regarding the results achieved in all the sections.

II. Test Image Selection

It is important to use a variety of images with different scenarios. These scenarios should be representative of the types of images that the codec (coder/decoder) is likely to transmit. Obviously there exists a large variety of images and one cannot accommodate all the different classes. For this thesis a subjective choice were made of typical pictures that the codec will come across, typically natural scenarios.

The United States database contains ten standard images and, at a recent conference [66], it was suggested that all images can be coded with four bits since these images were always used for evaluation purposes. The danger always exists that one can design an algorithm that is specific for a certain image or class of images. For practical purposes it was decided to use a selection of two images for the simulations presented in this thesis. In the experimental evaluation of algorithms other images were tested randomly to verify the results.

The images were chosen from natural occurring scenarios, the first image is called GIRL and the second image ROAD (see figures 2 and 3). The image GIRL contains the head and shoulders of a girl with a part of a room in the background. This image contains a good variety of textures and is typical of a video conference application. The second image, ROAD, was taken outdoors and contains a section of a road with vehicles travelling along the road. Some bushes and trees and other natural foliage as well as the typical horizon form part of the scenario. This image is typical of images that occur in remote sensing applications.

Figure 2 Original Image: GIRL (256x256x8)

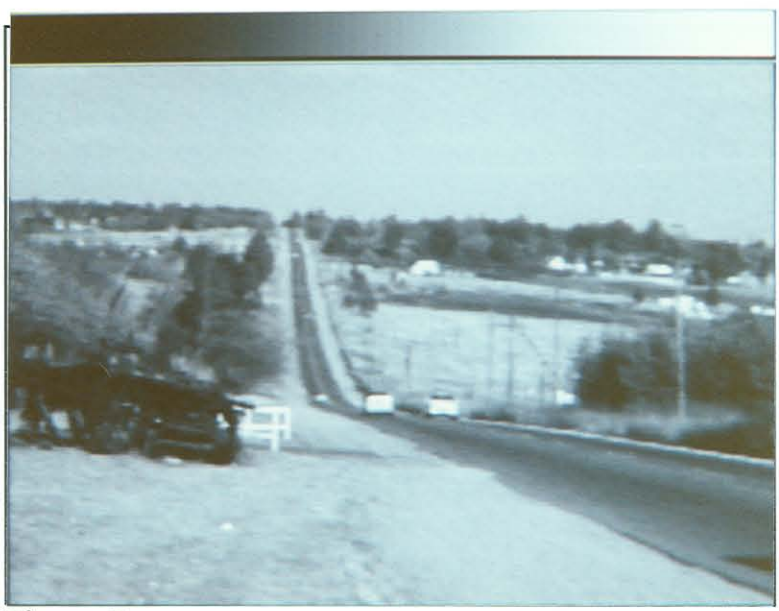

Figure 3 Original Image: ROAD (256x256x8)

III. Information Theory and Image Coding

Information theory provides us with mathematical tools to determine the channel capacity required to transmit a certain image or class of images over the channel. Two results from this theory give us a basis for image coding, they are [3]

$$0 \leq H(U) \leq \log_2(A) \tag{1}$$

and

$$H(U_N) \leq N H(U) \tag{2}$$

where H is the entropy function,

$$H(U) = -\sum_i p_i \log_2(p_i) \tag{3}$$

and U is a scalar source, U_N is an N dimensional source, p_i is the probability of source symbol u_i, and A is a source with uniform distribution. The first equation states that compression of the image data can be achieved if the statistical distribution of the data is not uniform, while the second equation states that further compression can be achieved if the data is dependant or correlated.

The theory behind these two equations together with the rate distortion theory form the basis of all image coding algorithms. Basically the above two equations determine that the output of the coder should consist of an independent uniformly distributed sequence while the rate distortion function determines the minimum distortion

at which this can be achieved for a fixed rate. The grey scale histogram of an image is normally not uniform, i.e. figures 4 and 5 show the histograms of the test images. By applying equation (1), the average bit rate can be computed for this image. Most images also contain a fair amount of correlation between the image pels. If a method could be devised to remove this correlation, equation (2) predicts a lowering in the average bit rate. In transform image coding the correlation is reduced by using an energy compacting transform. This property of the transform will be discussed in more detail in Section VII.

Information theory also provides the means by which to analyze, in a mathematical sense, the transmission of sources where some distortion of the source is acceptable. This is done in the framework of the *rate distortion theory*. A brief overview of the origin of the rate distortion function is given in the rest of this section. Most of the overview is based on the references [3] and [18].

The problem addressed by the rate-distortion theory is the minimisation of the channel capacity requirement while holding the average distortion at or below an acceptable level. More specific, the rate distortion function $R(D)$ is the minimum value of the mutual information $I(U,V)$ for a given distortion level D [3]. By keeping the rate lower than the channel capacity C, i.e $R(D)<C$, the possibility of obtaining distortion D is ensured.

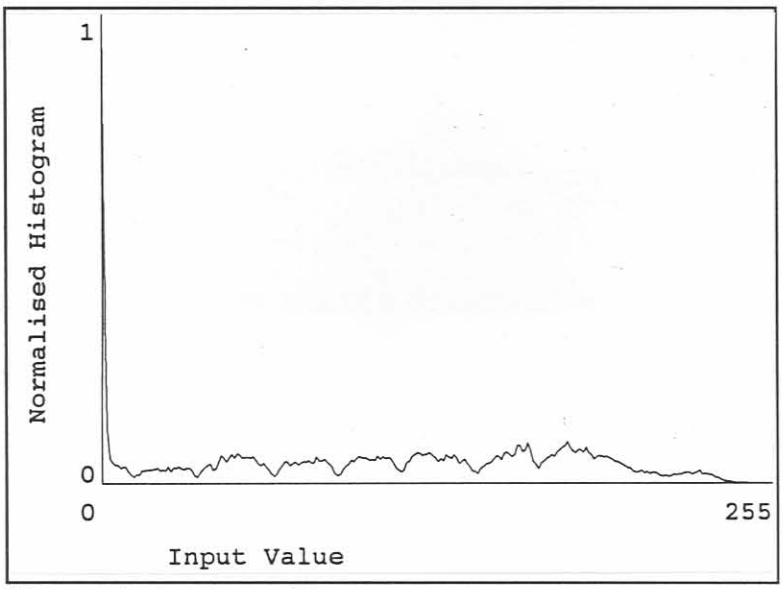

Figure 4 Histogram of the test image GIRL

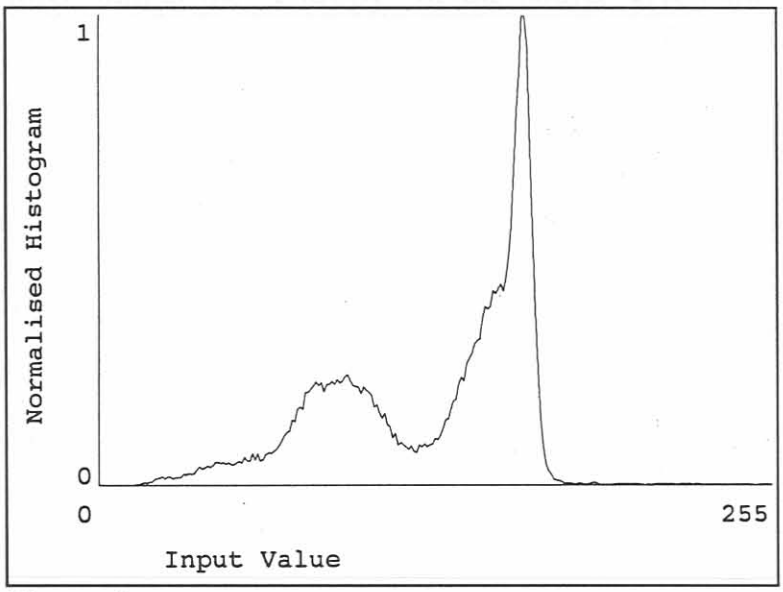

Figure 5 Histogram of the Image ROAD

The information theoretic measure of information transmitted is the average mutual information between U and V, and is defined for a block length N as:

$$I_N(U,V) = \sum_i \sum_j P(U_i) Q(V_j | U_i) \log \frac{Q(V_j | U_i)}{\sum_k P(U_k) Q(V_j | U_k)} \qquad (4)$$

Each block is described by one of a denumerable set of messages $\{U_i\}$ with probability $P(U_i)$. Any given system, i.e. channel, is described mathematically by the conditional probability $Q(V_j \ U_i)$ of message V_j being output by the decoder for a given source output U_i. The mutual information may also be written as

$$I_N(U,V) = H_N(U) - H_N(U|V) \qquad (5)$$

where $H_N(U \ V)$ is the entropy of the source given the observed decoder output. In other words the mutual information is equal to the entropy of the source minus the entropy of the source given the decoder output V.

If distortion is introduced then the decoder output only contains statistical information about U and as a result thereof $I_N(U,V)$ decreases. In the worst case V contains no information about U, so that $H_N(U \ V)=H_N(U)$ and $I_N(X,Y)=0$.

For the time discrete continuous-amplitude sources, the mutual information and average distortion functions are defined with integrals in place of the summations. Given the distortion $d(u,v)$ between u and v, the rate distortion results can be summarised as follows for block messages:

$$R(D^*) = \lim_{N \to \infty} \frac{1}{N} \inf_{q:D(q) \le D^*} I_N(U,V) \tag{6}$$

$$I_N(U,V) = \int p(u)q(v|u) \log \frac{q(v|u)}{t(v)} \, dv \, du \tag{7}$$

$$D(q) = \int d(u,v)\, p(u)\, q(v|u)\, dv\, du \tag{8}$$

$$t(v) = \int p(u)\, q(v|u)\, du \tag{9}$$

It is very difficult to solve these equations and it is normally only done for homogeneous, isotropic, Gaussian sources with a mean square error criterion. The rate for this particular Gaussian source is given by [18]

$$R(D^*) = \frac{1}{2} \log \frac{\sigma^2}{D^*} \quad for \quad \sigma^2 > D^* \tag{10}$$

The rate distortion theory is used in a later section to simulate the optimal encoding of images.

The next section looks at the statistical models used to facilitate a mathematical treatment of image coding.

IV. Image Statistical Models

Images are sometimes represented by simple stochastic models in order to develop useful algorithms or to compare the performance of various processes on an image mathematically. A stochastic process can be completely described by its joint probability density [1]. In general, high-order joint probability densities of images are usually not known, nor are they easily modeled [4]. For practical reasons the images are characterised by their mean and covariance functions.

A common model used, for natural images, is that of the two dimensional, stationary, first-order Markov process [1]. If f_{ij} represents the picture brightness at the point $(i\ ,\ j)$, then for this process the autocorrelation function may be written

$$R(m,n) = E[f_{ij}, f_{i+m,j+n}] = \rho^{|m-n|} \qquad (11)$$

$$where \quad 0 < \rho < 1$$

and zero mean is normally assumed $E[f_{ij}] = 0$. The assumption of zero mean is nonessential, since the mean can always be easily computed and subtracted if necessary to obtain a zero mean image.

To test the validity of the assumption the correlation of the two test images have been computed, horizontally and vertically, and is compared with the theoretical Markov model in figures 6 and 7. For large block sizes the images follow the model for small shifts from the origin.

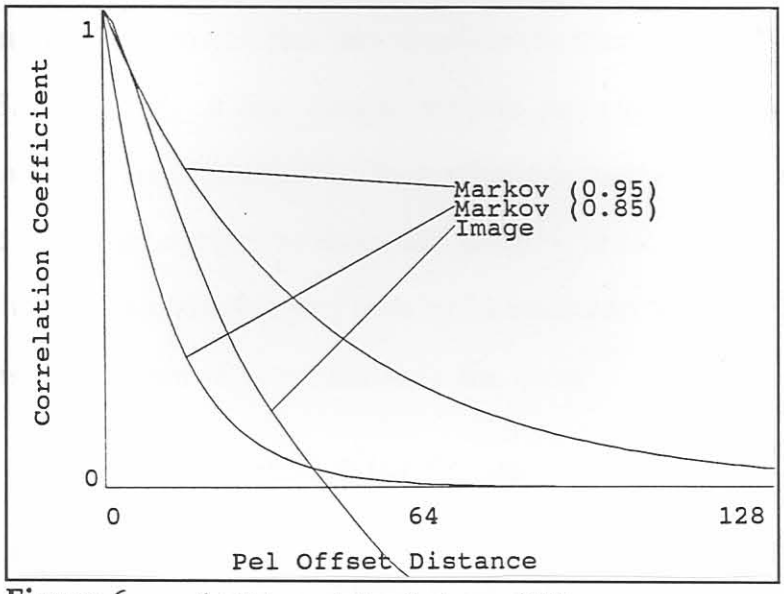

Figure 6 Spatial correlation for image GIRL

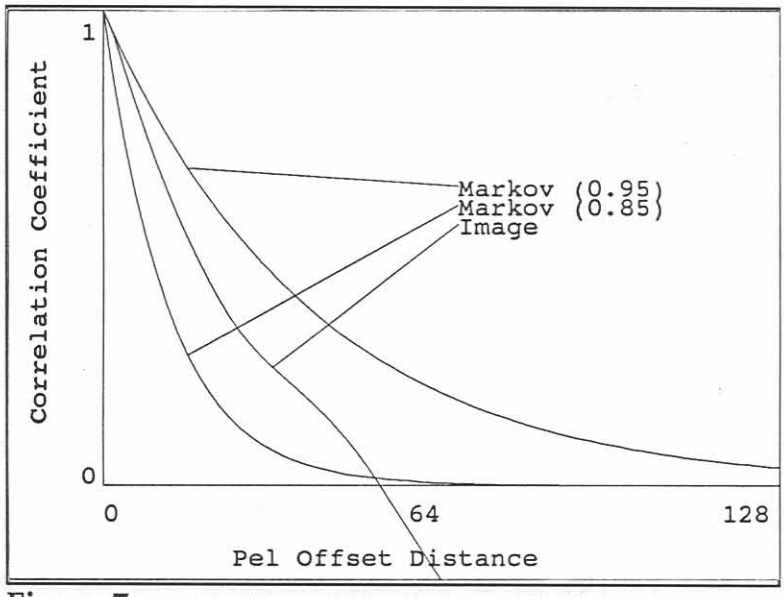

Figure 7 Spatial correlation for image ROAD

V. The Human Visual System

The human visual system (HVS) is a very complex system. At this time there is no accurate model that can simulate the visual interpretation of the HVS. However, a few simple models have been presented by various authors [16,21,22,23,27]. These empirical results were basically achieved by doing subjective threshold judging tests.

The results of the judging tests by Mannos and Sakrison [16] lead to a transfer function of approximately the form

$$A(f_r) \approx 2.6\ (0.0192+0.114\ f_r)\ \exp\ [-(0.114\ f_r)^{1.1}] \qquad (12)$$

where f_r is the radial frequency in cycles/degree. The equation has a peak value of one at 8 cycles/degree and diminishes at 64 cycles/degree. They also derived a nonlinear transfer function for the HVS given by

$$f(u) = u^{0.33} \qquad (13)$$

Plots of the two equations are given in figure 8.

A. Rate Distortion Simulation

To determine the best picture that any coding scheme may produce, the same rate distortion simulation procedure was followed that led to the generation of the empirical equations (12) and (13) [16]. To calculate the rate distortion function one must specify both the *distortion measure* and the *probability distribution* of the source. At present we are unable to specify the probability distribution of an image source. The best we can do is to specify the mean and correlation function for the image.

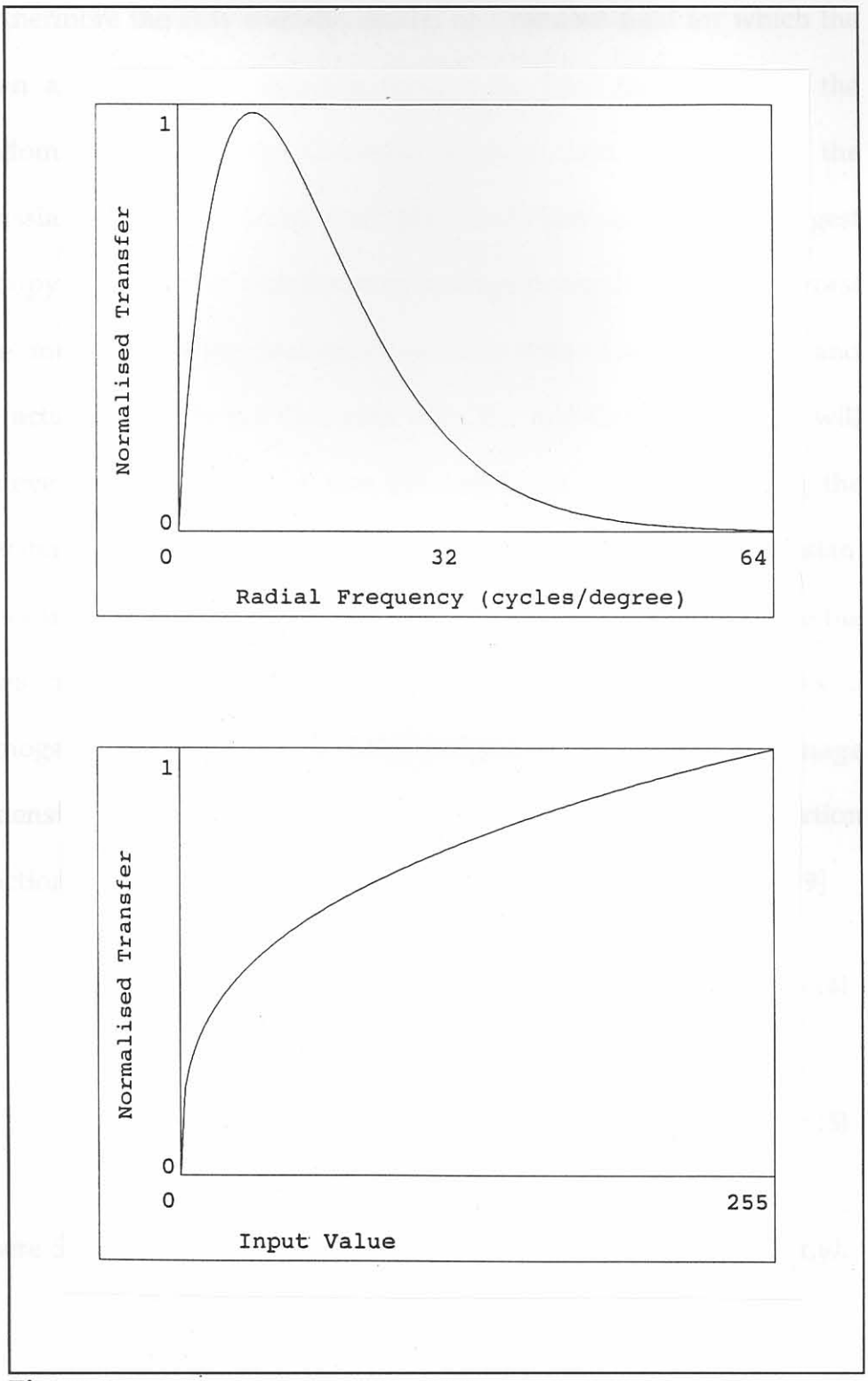

Figure 8 Transfer functions of the HVS

Furthermore the only tractable model of a random field for which the mean and correlation function specify the joint distribution of the random variables is the Gaussian random field. However, the Gaussian source is a "worst case" hypothesis because it has the largest entropy of all sources with the same average power [19,27]. This "worst case" means that if the simulations are done with a Gaussian model and the actual model is not Gaussian then the non-Gaussian source will achieve better results than was estimated. In transform coding the distribution of the errors in the spatial domain will be nearly Gaussian. This can be seen from the central limit theorem, i.e. the errors are the sums of independent errors in the transform coefficient. For a homogeneous (invariant to a shift in origin) Gaussian field with image dimension large compared to correlation distance, the rate distortion function is given in parametrical form by the pair of equations [19]

$$R(\mu) = \frac{1}{2} \iint_{S(f_x,f_y)>\mu} \log_2 [S(f_x,f_y)/\mu]\, df_x\, df_y \tag{14}$$

$$d^*(\mu) = \int_{-\infty}^{\infty}\int \min[S(f_x,f_y),\mu]\, df_x\, df_y \tag{15}$$

where $S(f_x,f_y)$ is the power spectral density of the input image $V(x,y)$.

If $V_{k,j}$ is the Fourier coefficients of $V(x,y)$, then those coefficients for which

$$E[|V_{k,j}|^2] \doteq \lambda_{kj} < \mu \tag{16}$$

are not transmitted. The remaining coefficients are transmitted in such a way that the received coefficients $B_{k,j}$ have a distribution such that $V_{k,j}$ - $B_{k,j}$ are Gaussian with zero mean, variance μ, and is independent of $B_{k,j}$. This can be simulated [16,19] by setting

$$B_{k,j} = \frac{\lambda_{k,j}-\mu}{\lambda_{k,j}} [V_{k,j} + N_{k,j}] \tag{17}$$

in which $N_{k,j}$ are zero-mean complex random variables, independent of $V_{k,j}$, and whose real and imaginary parts are uncorrelated. The variance of $N_{k,j}$ is given by

$$E[V_{k,j}^2] = \frac{\mu\lambda_{kj}}{2}(\lambda_{kj}-\mu) \tag{18}$$

The simulation then consists of the following steps:

1. Apply the nonlinear function (13) to the input image $u[x,y]$, i.e. $w[x,y]=f(u[x,y])$.
2. Compute the power spectral density $S_w[f_x,f_y]$ of $w[x,y]$ by using a smoothed periodogram technique, i.e. averaging the power spectral density computed from small overlapping sections of $w[x,y]$.

3. Weigh the power spectral density with the frequency sensitivity of the human visual system using (12), i.e.

$$S[f_r] = |A(f_r)|^2 S_w[f_r] \qquad (19)$$
$$where\ f_r = \sqrt{f_x^2 + f_y^2}$$

4. Using (14) iteratively, compute the μ corresponding to the desired rate.
5. Compute $W[f_x, f_y] = \text{FFT}\ \{ w[x,y] \}$.
6. Weigh W with the HVS (12), i.e. $V[f_x, f_y] = A(f_r)W(f_x, f_y)$.
7. Compute the variance of the coefficients $V_{k,j}$, i.e. apply equation (16), setting all coefficients with variance lower than μ equal to zero and adding noise according to (17) & (18) to the rest.
8. Compute the inverse FFT of B.
9. Apply the inverse of the HVS function (12) to the result of step eight.
10. Apply the inverse of the nonlinear function (13) to the result of step nine, this gives the rate distortion simulated picture.

It should be noted that no provision has been made to accommodate overheads in the average bit rate using this simulation, i.e. coding the position of coded coefficients. To avoid this problem and to keep the class of images as wide as possible, the simulations were done using the first order Markov model. The power spectral density for this model is given by (Appendix D),

$$S(\omega) = 2\sigma^2 \cdot \frac{\alpha}{\alpha^2 + \omega^2} \qquad (20)$$

where σ^2 *is the image variance,*

and where the correlation $\rho = e^{-\alpha}$

The simulation results are shown in figures 9 and 10. The results show that very good quality images are possible for bit rates of 1.0 and 0.5 bits/pel. These pictures can now be compared to those produced by the actual codec. Based on the comparison one should be able to decide how much more can be done to improve the codec performance. For example one would be able to determine if the added complexity is worth the gain in image quality. The next paragraph looks at the range of frequencies for which (12) is valid in normal viewing situations.

Figure 9 Rate Distortion Simulation: GIRL rate=1 bit/pel.

Figure 10 Rate Distortion Simulated Image: GIRL rate=0.5 bit/pel.

B. Parameters for the HVS

To apply (12) to the images used in this simulation it is necessary to compute the frequency range for which it is valid. This can be done by examining the system in figure 11. From this figure it is easy to determine that the angle spanned by the viewing device is given by the relationship

$$\theta = 2 \tan^{-1}\left(\frac{r}{d}\right) \tag{21}$$

where d is the distance from the screen, and $2r$ is the size of the screen. For a distance from the viewing device of 50cm and a *horizontal* screen size of 7.2" (9" diagonal) the horizontal viewing angle is 20.73 degrees. For an image resolution of 256 pels horizontally, the maximum number of cycles would be 128, which gives a frequency of 128/20.73 = 6.18 cycles/degree.

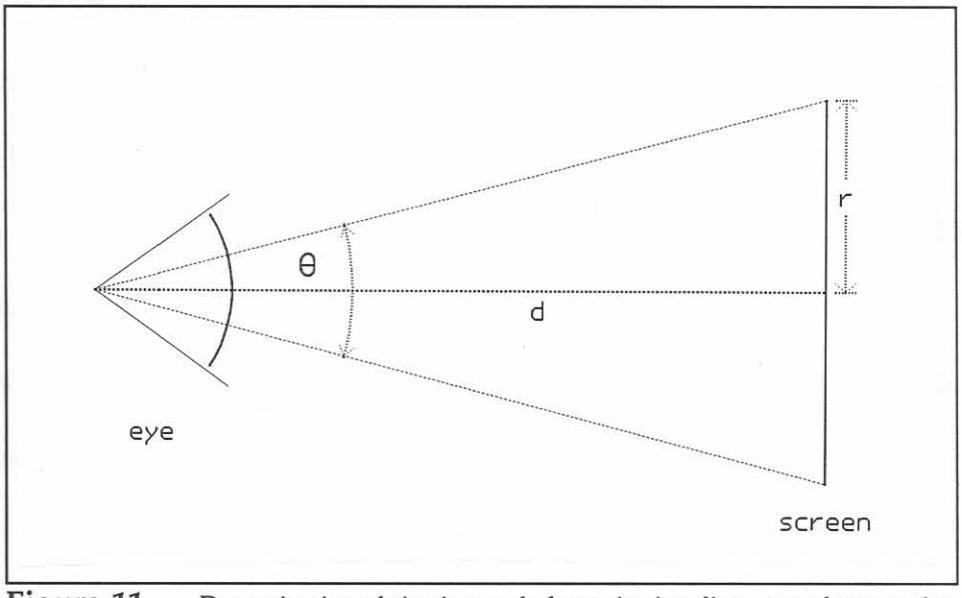

Figure 11 Determination of viewing angle from viewing distance and screen size.

A few different viewing angles have been computed for changing viewing distances and screen sizes, and are given in table I. From this table it is clear that the frequency response of an image, with resolution of 256x256, displayed on a device with the given physical parameters is lacking in comparison with the resolution ability of the human eye (64 cycles/ degree).

Viewing Distance	Horizontal Screen Size		
	4" Photo (5" diag.)	7.2" (9" diag.)	11.2" (14" diag.)
30cm	6.66	3.78	2.52
50cm	11.03	6.18	4.03
1m	22.01	12.25	7.91
2m	43.99	24.45	15.73

Table I Maximum normalised frequency available from different viewing devices for an image resolution of 256x256

For images with a resolution of 512x512 pels the frequency response will be exactly double that shown in the table.

The next section introduces the distortion measures that will be used to determine image quality in a more mathematical sense. It should be kept in mind that a subjective evaluation of the image coding results should be used as final evaluation measure.

VI. Image Quality

A very important part of the design of a high quality image coder is the evaluation of the performance of different algorithms inside the image codec itself. To do this it is necessary to specify a fidelity criterion, i.e. some measure by which we can determine the quality of the reconstructed image. The mean square error is frequently used in image processing applications. It is defined as follows for images

$$e_{ms}^2 = \frac{1}{N^2} \sum_{x=0}^{N-1} \sum_{y=0}^{N-1} (i(x,y) - o(x,y))^2 \qquad (22)$$

where the input pels are designated by i, and the output pels are designated by o. There are two definitions of signal to noise ratios (SNR) which use the definition of the above error. The first is the normalised signal to noise ratio

$$NSNR = 10 \; Log_{10} \frac{\sigma^2}{e_{ms}^2} \qquad (23)$$

where σ^2 is the variance of the original image. The second definition is that of the peak signal to noise ratio (PSNR), defined as

$$PSNR = 10 \; Log_{10} \frac{(255)^2}{e_{ms}^2} \qquad (24)$$

Although the mse measure does not agree with subjective evaluations of coded images, the mse gives an indication of the physical accuracy of reconstruction, and as such it is a useful measure.

The mse measure indicates the accuracy of both subjectively-important and subjectively-redundant image reconstruction. It has been found from experience that the mse only starts to fail as a good measure when the signal to noise ratio is relatively low, i.e. when coding of subjectively redundant information cannot be tolerated. Since this is normally the case for bit rates below one bit per pixel, a HVS frequency response weighted mse measure will also be used. This measure was also used by Davisson [18], and is defined as follows: If I_f is the spectrum of the input image and O_f is the spectrum of the reconstructed image then the weighted mse (wmse) is given by

$$e_{wms}^2 = \frac{1}{N^2} \sum_{x=0}^{N-1} \sum_{y=0}^{N-1} \left| A_f(x,y) \right|^2 \left(I_f(x,y) - O_f(x,y) \right)^2 \qquad (25)$$

where A_f is the frequency response of the HVS given by (12). The HVS was implemented for a nine inch diagonal viewing device viewed from half a metre. From table I the maximum observable frequency would then be 6.18 cycles/degree. This would mean that the HVS frequency response would be that of a high pass filter.

The next section examines the basic transform image codec structure. It gives a description of all the different sections, gives results of images coded with this codec and then proceeds to an analysis of the origins of the errors in transform coding.

VII. Basic Transform Image Coding Structure

For the high quality coding and transmission of still pictures one needs to exploit all structure or redundancy present within the image. Transform image coding has been found to be a robust and efficient way to achieve this [1,4,5,6,7,61,62]. This section starts with a brief overview of the structure of a typical intraframe codec, which is followed by a more detailed discussion of the different aspects involved.

In transform coding the image is first decorrelated by using a suitable transform. This step is normally reversible and contributes little to the overall image degradation, except for round-off errors in integer implementations. With a suitable transform the decorrelation step can achieve efficient energy compacting, as will be discussed in more detail in a following section.

The next step involves the quantisation of the coefficients, and it is in this step that the actual image compression takes place. This step is *irreversible* and is responsible for the majority of degradation in the reconstructed image. The statistics of the coefficients are normally exploited in the quantisation step to minimize the distortion.

The last step is channel encoding, and involves adding some redundancy to minimise the effect of channel errors. This step is important because of the efficient representation of the image data, which implies that a small error might have a significant influence on

the output image. The decoder section at the receiver starts with channel decoding followed by a reconstruction of the coefficients and an inverse transform.

The next section will look at the selection and desirable properties of the transform to make the transform coding as efficient as possible.

A. Transforms

A truly optimum transform would result in the best picture quality using the least number of bits. This is a criterion which is difficult to specify quantitatively. A simpler criterion is to require that the transform coefficients be statistically independent, but this requires knowledge of the probability density function of images which we do not yet have. Using second order statistics we can find a transform that results in uncorrelated coefficients. From the view of the information theory (see equation 2), the transform attempts to decrease the entropy of the image by taking advantage of dependencies in the source.

A significant unitary transform is the Karhunen-Loeve transform (KLT) for random fields. It is the complete orthonormal set of basis images $b(.)$ determined from the eigenvalue equation

$$\sum_m \sum_n r(k,l;m,n)\, b(i,j;m,n) = \lambda_{i,j}\, b(i,j;k,l) \qquad (26)$$

where $r(.)$ is the image covariance function.

The optimality of the KLT for image processing stems from the following two properties [51]:

1. It completely decorrelates the transform coefficients, i.e.

$$Cov\,[v_{k,l}(T), v_{m,n}(T)] = \sigma^2_{k,l}(T)\,\delta_{k,m}\delta_{l,n} \quad for \quad T=\Phi \qquad (27)$$

where T denotes an arbitrary N^2xN^2 unitary transform, Φ is the KLT and $\sigma^2(T)$ is the variances of the T-transform coefficients $v(T)$.

2. Compared to all other unitary transforms, the KLT packs the maximum expected energy in a given number of samples, say M, i.e.

$$\sum_{k,l \in S(\Phi)} \sum \sigma^2_{k,l}(\Phi) \geq \sum_{k,l \in S(T)} \sum \sigma^2_{k,l}(T) \quad \forall \quad 1 \leq M \leq N^2 \qquad (28)$$

where $S(T)$ is the set containing M index pairs (k,l) corresponding to the largest M variances in the T-transform domain. This property serves as a basis for transform data compression techniques.

Although the optimal transform is explicitly known, its use in practice results in problems such as:

* Different basis functions for every class of images as a result of the non-stationarity of images,
* Singularities may exist in the covariance matrixes which means that all the basis functions cannot be computed,
* No fast transform exist for the KLT.

For the Markov image model as described in section IV the discrete cosine transform (DCT) has been found to be very similar to the KLT, and can be derived as the limiting case of the KLT as the correlation coefficient approaches one, i.e. $p \rightarrow 1$. The DCT has also been found to perform better than other transforms in many image coding applications [36,40,41,45]. The DCT does not perform well for negative correlations or for correlations below 0.5.

The forward DCT is defined by Ahmed, Natrajan and Rao [31]:

$$F(u) = \frac{2\,c(u)}{N} \sum_{j=0}^{N-1} f(j) \cos\left[\frac{(2j+1)\,u\,\pi}{2N}\right];$$

$$u = 0,1,\ldots,N-1$$

where

$$c(u) = \frac{1}{\sqrt{2}} \quad \text{for } u = 0$$

$$c(u) = 1 \quad \text{for } u = 1,2,\ldots,N-1$$

$$c(u) = 0 \quad \text{elsewhere.}$$

(29)

and the inverse transform is

$$f(j) = \sum_{u=0}^{N-1} c(u)\,F(u) \cos\left[\frac{(2j+1)\,u\,\pi}{2N}\right]$$

$$j = 0,1,\ldots,N-1$$

(30)

Since the DCT is separable, the two dimensional transform can be computed by transforming the rows of the image followed by transforming the columns using the one dimensional transform. Many fast algorithms has been proposed for the DCT [31,32,33,34,35,37].

Normally the whole image is not transformed in a single transform since the statistics in an image is highly spatially variant, and from the information theory it would be better to group areas of similar statistics together. Coding images using a full-image transform normally results in a loss of detail, it is also time consuming, requires a large amount of memory, and require higher precision mathematical

processors. This leads to the *spatially adaptive* quantisation that will be discussed in the next section.

1. Transform Block Size

The question that remains is that of block size. In real images the assumption of a Markov model are not valid especially if the block size is small [7]. Computer simulations on real pictures show [7] that the mean square error (mse) produced by transform coding improve with the size of the sub-picture, but it does not improve meaningfully beyond 16x16. Natrevali [7] also showed that the subjective image quality does not appear to improve much with block size beyond 4x4.

To determine the influence of block size on the image quality, the test images were coded to 1.0 bits/pel for block sizes 4x4, 8x8, and 16x16. The coefficients were coded using a Laplacian pdf optimised Lloyd-Max quantiser with optimal bit assignment for mean square error minimisation. A graph of peak signal to noise ratio versus block size is given on figure 12. Figures 13 to 15 contains the coded image results for the different block sizes. The signal to noise ratio (S/N) increased with an increase in block size. The difference in S/N decreases between successive block sizes as the block size increases. The 4x4 block size showed a noticeable vector quantiser type noise along edges in the image. There were little difference, in subjective image quality, between transform block sizes of 8x8 and 16x16. Most of the simulations done further on in the thesis will use a block size of 8x8.

The reasons being that it allows for better adaption to local statistics, and also because DCT-chips exist that can do 8x8 transform in real time. The existence of the DCT-chips probably means that most of the current real world systems will use this block size.

Since the quantisation forms such an important section of the coder structure, it will be discussed in a separate section. The following section will investigate the different approaches that is used in the quantisation of the transform coefficients.

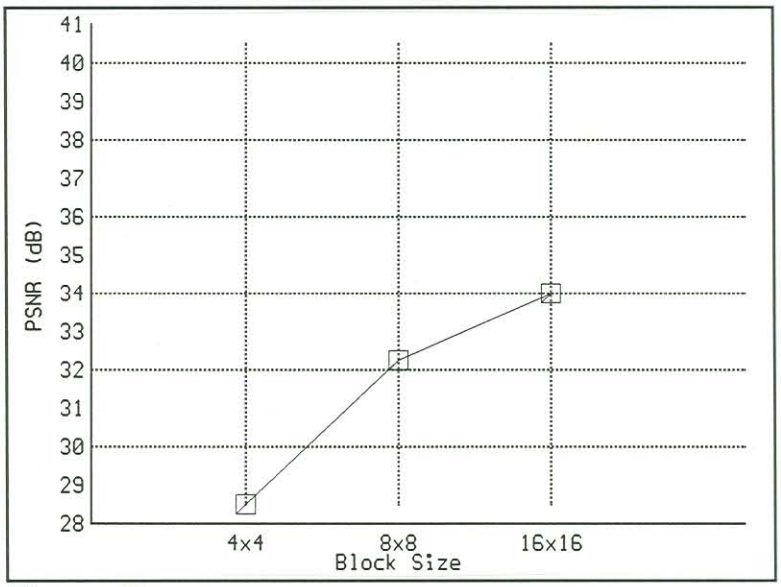

Figure 12 Signal to Noise Ratio versus Block Size for the image GIRL coded to 1.0 bits/pel.

Figure 13 GIRL coded using a DCT of size 4x4, 1.0 bits/pel.

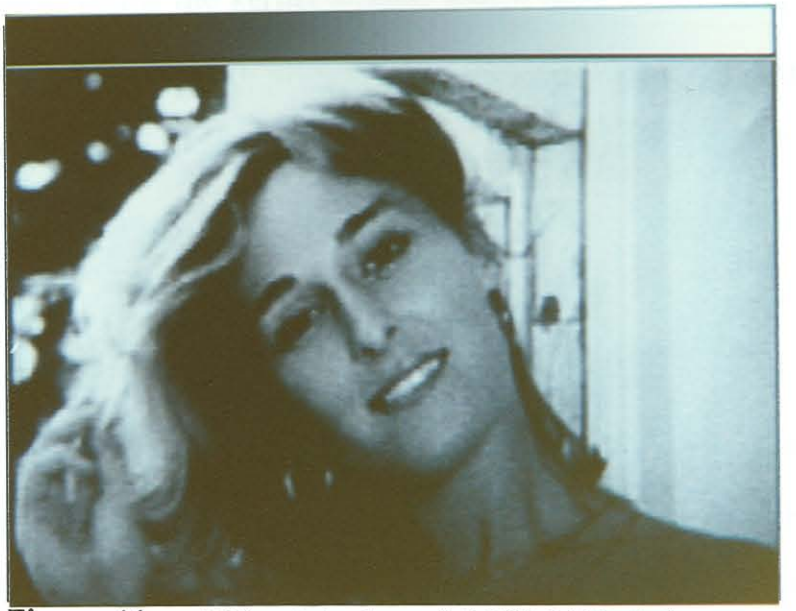

Figure 14 GIRL coded using an 8x8 DCT, 1.0 bits/pel.

Figure 15 GIRL coded using a 16x16 DCT, 1.0 bits/pel.

VIII. Quantisation

Quantisation forms the kernel around which most of the compression revolves once the transform has been chosen. From the information theory guidelines this section is equivalent to solving (1), and sometimes both (1) and (2). The input of the image codec is assumed to be already digitised with a sufficient number of bits per pixel (6 bits or more for normal monochrome video systems) to avoid contouring effects. As a result of the mathematical processing in the transform, the dynamic range of the transform coefficients is much more than that of the spatial image. The larger the block size the bigger the dynamic range of the coefficient since there are more multiply and adds. The coefficients need to be quantised further in order to achieve the desired compression ratio. The quantisation of the coefficients will be investigated in this section. The first part of this section deals with the actual quantiser design while the second part is concerned with the optimal allocation of bits to each coefficient.

Since the dynamic range of the coefficients is bounded the distribution of the coefficients is always bounded between absolute maximum and minimum values. These values are determined by the dynamic range of the input signal and the type of transform used. For an orthonormal real transform the maximum and minimum values are half (since the input is positive and the basis-function norm is one) that

of the maximum value of the input signal times a constant that is proportional to the size of the transform.

Three different types of quantisation will be investigated. The first is the Lloyd-Max quantiser that has been frequently used and still is very popular for use in image coding systems. This quantiser makes use of the probability density function (pdf) of the coefficients to iteratively minimise the mean square error. The second set of quantisers are more simple and are classified as companders. As the name indicates they make use of a nonlinear function derived from the pdf to transform the coefficient to a uniform distribution where it can be quantised uniformly. Both of these quantisers operate on a sample by sample, i.e scalar, basis. The third method of quantisation that will be looked at is that of source coding. In source coding the coefficients are quantised uniformly and then coded via an optimal source encoding scheme like Huffman coding.

A. Lloyd-Max Quantisers

Quantisation [1,57] is the process of subdividing the range of a signal into non-overlapping regions. The amplitude of the signal is compared to a set of decision levels. If the sample amplitude falls between two decision levels, it is quantised to a fixed reconstruction level lying between the two decision levels. The quantiser as defined here is a memoryless non-linearity and is shown graphically in figure 16.

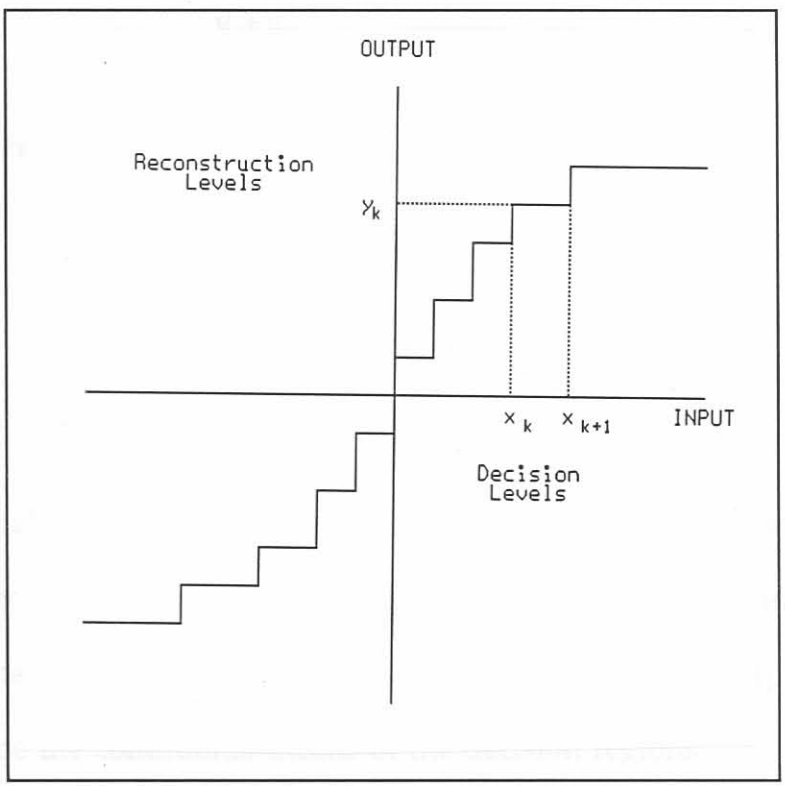

Figure 16 Quantiser input output characteristic.

Consider an N level quantiser with output levels $y_1, y_2, \ldots, y_N$. The output level y_k is associated with a decision region specified by its boundaries, the decision levels,

$$y_k \Leftrightarrow < \{x_{k-1} < x \leq x_k\}, \quad for \quad k = 1,2,\ldots,N. \tag{31}$$

For convenience, the x_i are in increasing order and the two extreme decision levels, x_0 and x_N, are chosen at infinity.

The total mean square error (mse) is

$$\overline{e^2} = \sum_{i=1}^{N} \int_{x_{i-1}}^{x_i} (x - y_i)^2 \, p(x) \, dx \tag{32}$$

Differentiating the mse with respect to x_k and y_k and setting equal to zero gives the decision levels as

$$x_k = \frac{y_k + y_{k+1}}{2}, \quad for \quad k = 1,2,\ldots,N-1 \tag{33}$$

and the reconstruction levels as

$$y_k = \frac{\int_{x_{k-1}}^{x_k} x \, p(x) \, dx}{\int_{x_{k-1}}^{x_k} p(x) \, dx}, \quad for \quad k = 1,2,\ldots,N \tag{34}$$

These conditions must be satisfied by a minimum mean square error quantiser. They can be interpreted to mean that the decision levels should be midway between the output levels and that the output levels should be the conditional means of the decision regions.

Recursive solution of equation (33) and (34) for a given pdf provides the values for the optimum decision and reconstruction levels. Two versions of the iteration that can be used is given in [57]:

Method I

In the first version, often termed Lloyd's method I, an initial guess is made for the output levels and a set of decision boundaries corresponding to these is determined using (33). Then (34) can be applied to determine a new set of output levels which is optimal for the decision boundaries just determined, completing one iteration. At the end of an iteration the mse has either decreased or remained unchanged.

A variation of this technique, introduced by Kabal [57], applies both halves of the iteration to each output level in turn. In this way the effect of changing an output level is allowed to propagate to other output levels. This modified version of method I, which uses the same number of integral evaluations as the original technique, often converges faster in practice. This method was used for the computation of the Max-Lloyd quantiser levels in this thesis, and no problems with convergence were experienced.

Method II

A variational technique, dubbed method II, proposed by both Lloyd and Max involves a one dimensional search. An initial guess is made as to the value of the first output level y_1. The

The Lloyd-Max quantiser was implemented for the Laplacian density function

$$p(x) = \frac{\alpha}{2} e^{(-\alpha|x|)} \qquad (35)$$

$$where\ \alpha = \sqrt{\frac{2}{\sigma^2}}\ ,\ \sigma^2\ is\ the\ variance\ of\ x$$

The reconstruction levels can be solved by replacing (35) in (34), i.e.,

$$y_k = \frac{(\alpha x_k + 1)\, e^{-\alpha x_k} - (\alpha x_{k-1} + 1)\, e^{-\alpha x_{k-1}}}{\alpha\, e^{-\alpha x_k} - \alpha\, e^{-\alpha x_{k-1}}} \qquad (36)$$

The mean square error can be computed by replacing (35) in (32), i.e.,

$$err_i^2 = \int_{x_{i-1}}^{x_i} (x^2 - 2xy_i + y_i^2)\, \frac{\alpha}{2}\, e^{(-\alpha x)}\, dx \qquad (37)$$

this reduces to

$$err_i^2 = f(x_i) - f(x_{i-1})$$

$$where \qquad (38)$$

$$f(x) = e^{-\alpha x} \left(\frac{y(x+1)}{\alpha} - \frac{y^2}{2} - \frac{(\alpha x)^2 + 2x + 2)}{2\alpha^2} \right)$$

The average mse is given by

$$\overline{err^2} = \sum_{i-1}^{N} err_i^2 \qquad (39)$$

This error function has been tabulated in the *bit-assignment* section, Table II. The recursive solution of method I has been used for computing the decision and reconstruction levels. It was found that this method converged quickly for quantiser sizes up to eight bits.

value of the decision level below this output level, in this case x_0, is known. The next decision level can be determined by finding the value of x_1 which satisfies (34). This step is normally carried out using iterative numerical techniques. The next output level can now be computed and the process repeated for all levels. The last output level will generally not be the conditional mean of the last interval. The difference between y_N and the conditional mean of the last interval can be used to determine an update for y_1 for the next iteration. The process of determining the output levels continues until sufficient precision has been achieved.

For the mse, a sufficient condition for uniqueness of the Lloyd-Max solution is log-concavity of the pdf [57]. The Gaussian and Laplace distributions have associated with them unique (and hence symmetrical) quantisers. It is also shown [57] that the Laplace distribution occupies a unique place in the continuum of generalized Gamma distributions in that it sits on the boundary between distributions that have unique optima and those which do not.

Conversion was slow for higher bit rates as a result of the increase in number of levels that had to be computed for every iteration.

All numerical implementations involving this kind of recursive structure with mathematical functions, were done using double precision mathematics. The decision and reconstruction levels generated were verified with those given by Pratt [1 p.144].

A different approach to nonlinear quantisation that achieves similar results is that of companding (compressing and expanding) a signal and using uniform quantisation. The compander quantiser is discussed in the next paragraph.

B. Companders

A compander (compressor-expander) is a uniform quantiser preceded and succeeded by nonlinear transformations as shown in figure 17. The random variable x is first passed through a nonlinear memoryless transformation $g(.)$ to yield another random variable w. This random variable is uniformly quantised to give $y\varepsilon\{yi\}$, which is non-linearly transformed by $h(.)$ to give the output z. The overall transformation from x to z is a nonuniform quantiser. The functions $h(.)$ and $g(.)$ can be easily derived:

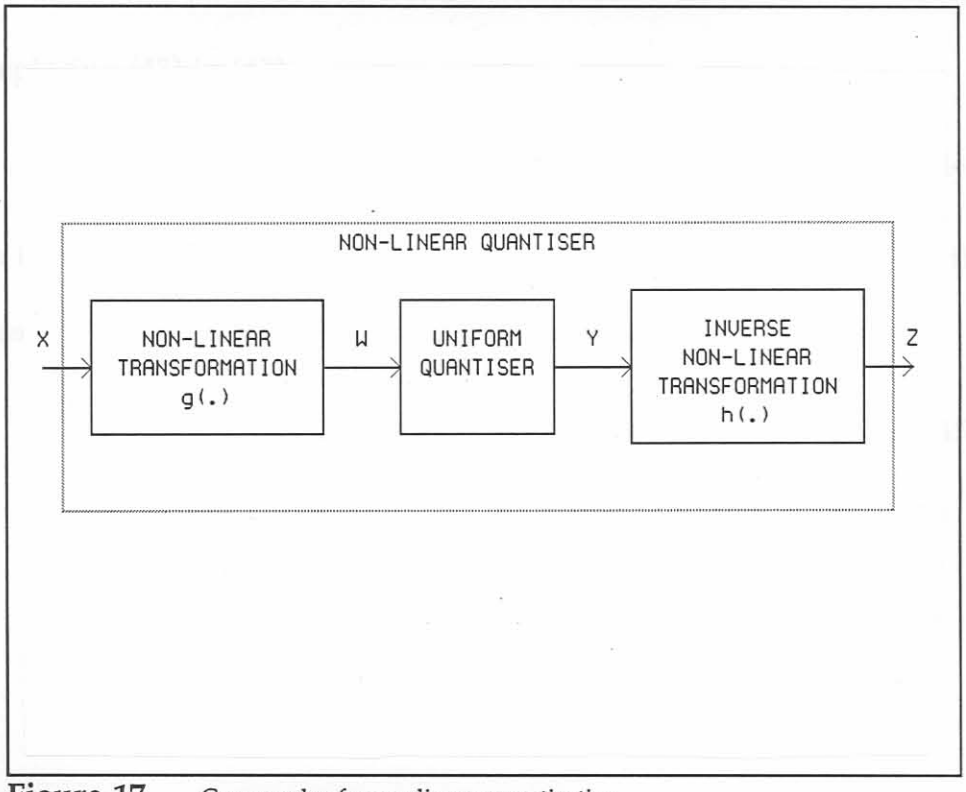

Figure 17 Compander for nonlinear quantisation

We wish to find a function $g(x)$ such that the random variable

$$Y = g(X) \tag{40}$$

transforms the input cumulative distribution function (cdf) $F_X[x]$ to a desired output cdf $F_Y[y]$. The cumulative distribution function is a monotone increasing function, that is

$$F_X[x_1] \leq F_X[x_2] \quad if \quad x_1 \leq x_2 \tag{41}$$

Since $Y=g[X]$, we have

$$P\{Y \leq y\} = P\{X \leq x\} \tag{42}$$

where P is the probability of occurrence.

From the left hand side in (42) and using (40) we have

$$F_Y[y] = P\{Y \leq y\} = P\{g(X) \leq g(x)\} \tag{43}$$

Replacing (43) in (42)

$$F_Y[g(x)] = F_X[x] \tag{44}$$

In (44) $f_X[x]$ is the pdf of the input to the quantiser and $f_Y[g(x)]$ is the desired pdf. The function $g(x)$ can be computed by inverting (44)

$$g(x) = F_Y^{-1}[F_X[x]] \tag{45}$$

For a uniform output pdf, between maximum and minimum values $f_Y(y)$ becomes

$$f_Y(y) = \frac{1}{y_{max} - y_{min}} \tag{46}$$

Substituting (46) into (45) gives

$$g(x) = (y_{max} - y_{min}) F_X[x] + y_{min} \tag{47}$$

The expansion is done by computing the inverse of this function, i.e.

$$h(z) = g^{-1}(x) \quad with \quad z = g(x) \tag{48}$$

The performance that can be achieved with the compander and the Max-Lloyd quantiser is similar [4]. However, the compander is simpler to compute and easier to implement for common distributions, i.e. the Laplacian distribution. As an example of the application of equations (47) and (48) the forward and inverse transformation functions were computed for the Laplacian distribution, the derivation is given in Appendix B. Other companders, i.e Gaussian and Rayleigh, are given by Pratt [1].

C. Source Encoding

For source coding the entropy of the output sequence is specified, if the distribution of the input is known this allows us to compute the step size of the quantiser. For ease of implementation the uniform quantiser is normally used [57]. The uniform quantiser with source coding is normally a sub-optimal quantiser, except for the Laplacian distribution, for which it is the optimum quantiser [53,57,59].

A method to compute the optimal bin width is given by Eggerton and Sirnath [56]. They determined the entropy of the quantised coefficients to be approximately given by, (see Appendix C)

$$H(x^*) = H(x) + \beta\Delta - \log_2\Delta$$

$$\textit{where}\quad \Delta = \textit{stepsize},$$

$$\beta \quad \textit{is a function of the variance},$$

$$H(x) \textit{ is the entropy of the source.} \tag{49}$$

If the coefficients are assumed to be Laplacian distributed, the variables of (49) was found to be [57]

$$H(x) = \log_2(\sqrt{2}\,\sigma e)\,\log_2 e \qquad (\textit{bits})$$

$$\beta \simeq \frac{0.096}{\sigma} \tag{50}$$

$$\textit{where } \sigma \textit{ is the standard deviation}$$

The bin width can now be obtained from (49) by equating $H(x^*)$ with the desired bit rate. Once the coefficients have been quantised, an optimal source encoding method, i.e. Huffman coding, can be used.

The uniform quantiser with source coding were used in simulations on the test image's. A comparison between the Lloyd-Max quantiser and the source encoding quantiser is given in figure 18, with the results for images coded with 2.0, 1.0 and 0.5 bits/pel given in figures 19-21. It is clear from the graph that the source coder performs better than the Lloyd-Max quantiser. This is in agreement with theoretical predictions [7].

For efficient quantisation, it has been shown in the discussion regarding the quantisers, that knowledge of the coefficient density functions is necessary. The next paragraph investigates the different functions that has been proposed in the literature.

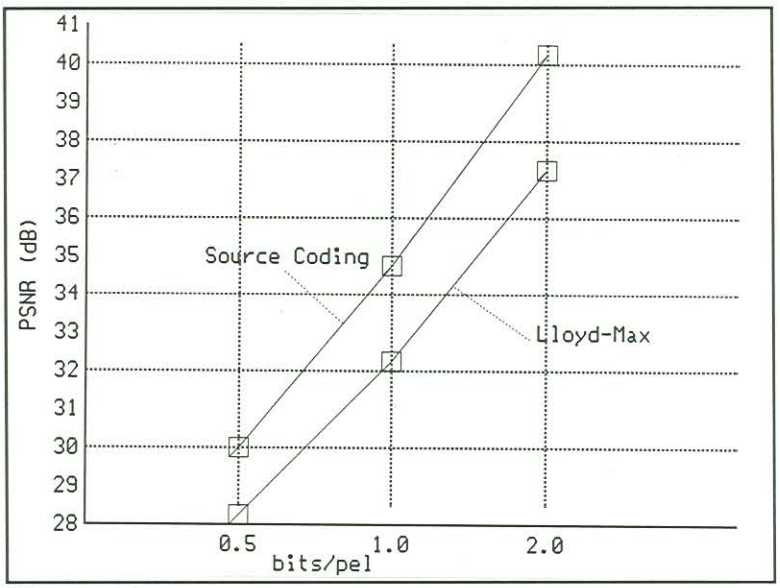

Figure 18 Comparison of the performance of the Source Encoder versus the Lloyd-Max quantiser. Transform=DCT (8x8)

Figure 19 The image GIRL DCT coded to 2.0 bits/pel, using uniform quantisation with source encoding.

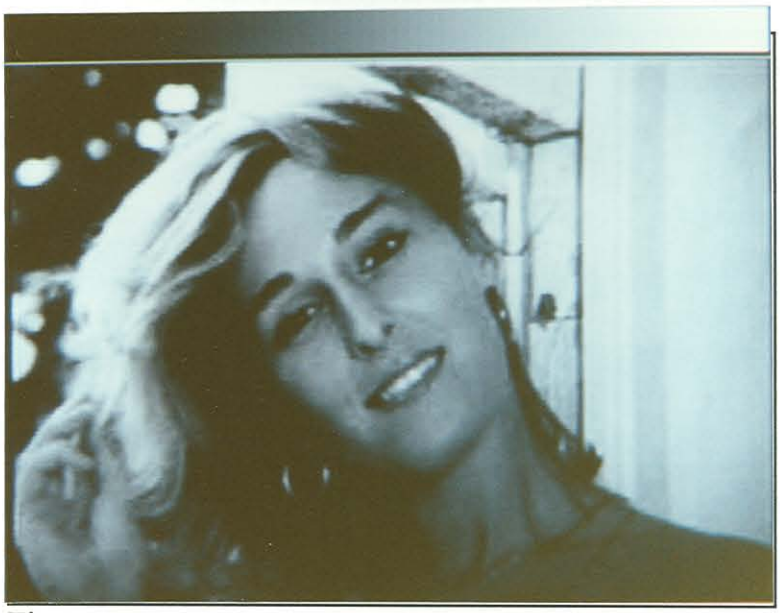

Figure 20 The image GIRL DCT coded to 1.0 bits/pel, using uniform quantisation with source encoding.

Figure 21 The image GIRL DCT coded to 0.5 bits/pel, using uniform quantisation with source encoding.

D. Coefficient Statistics

After the image has been subdivided into a number of smaller blocks, to take advantage of the spatial variant nature of images, these blocks are transformed using the DCT or a similar transform to decorrelate the images. The different coefficients, of similar index, are then grouped together and quantised using one of the quantisation methods just described. Since all of these methods need to know the distribution of the coefficients a priori, in order to determine decision levels or to achieve a certain rate, the determination of a representative distribution is important.

Several distributions have been suggested by various authors. Pratt [1] suggested that the DC coefficient should have a Rayleigh distribution since it was the sum of positive values, and that, based on the central limit theorem, the other coefficients should be Gaussian. Netravali and Limb [7] agreed with the above assumption and also stated that the histogram of non DC coefficients were roughly bell-shaped. On the other hand, some authors [30] thought that the non-DC coefficients were not Gaussian, but Laplacian. A few authors agreed that the DC coefficient was Gaussian. These different assumptions have led Reininger and Gibson [30] to perform goodness-of-fit tests on the transform coefficients in order to identify the distribution that best approximates the statistics of the coefficients. In the tests they considered the Gaussian, Laplacian, Gamma, and Rayleigh distributions. The test that they used was the well-known

Kolmogorov-Smirnov test. The results of their paper indicate that for a large class of images, the DC coefficient is best modeled by a Gaussian distribution, and the non-DC coefficients are best modeled by the Laplacian distribution.

The histograms of the coefficients of the two test images were computed, see figure 22. The results shown in figure 22 were for the coefficient [1,1] as well as the DC coefficient. The images were transformed with an 8x8 DCT transform. The results show that the non-DC coefficients were Laplacian distributed as experimentally determined. The DC coefficient could however not be described as anywhere near Gaussian, but it is recognised that a larger database was used in [30]. It was decided to code the DC-coefficient using a uniform distribution and the other coefficients using a Laplacian distribution. The next paragraph will investigate the question as to which coefficients should be coded and how many bits should be used for every coefficient.

E. Bit Assignment

Bit assignment is normally discussed in the literature under Block quantisation. Block quantisation is an efficient scheme to quantise a block of independently distributed random variables. In block quantisation each element of a vector is quantised on an element by element basis. These elements are normally not quantised equally well as will become clear in the following paragraph.

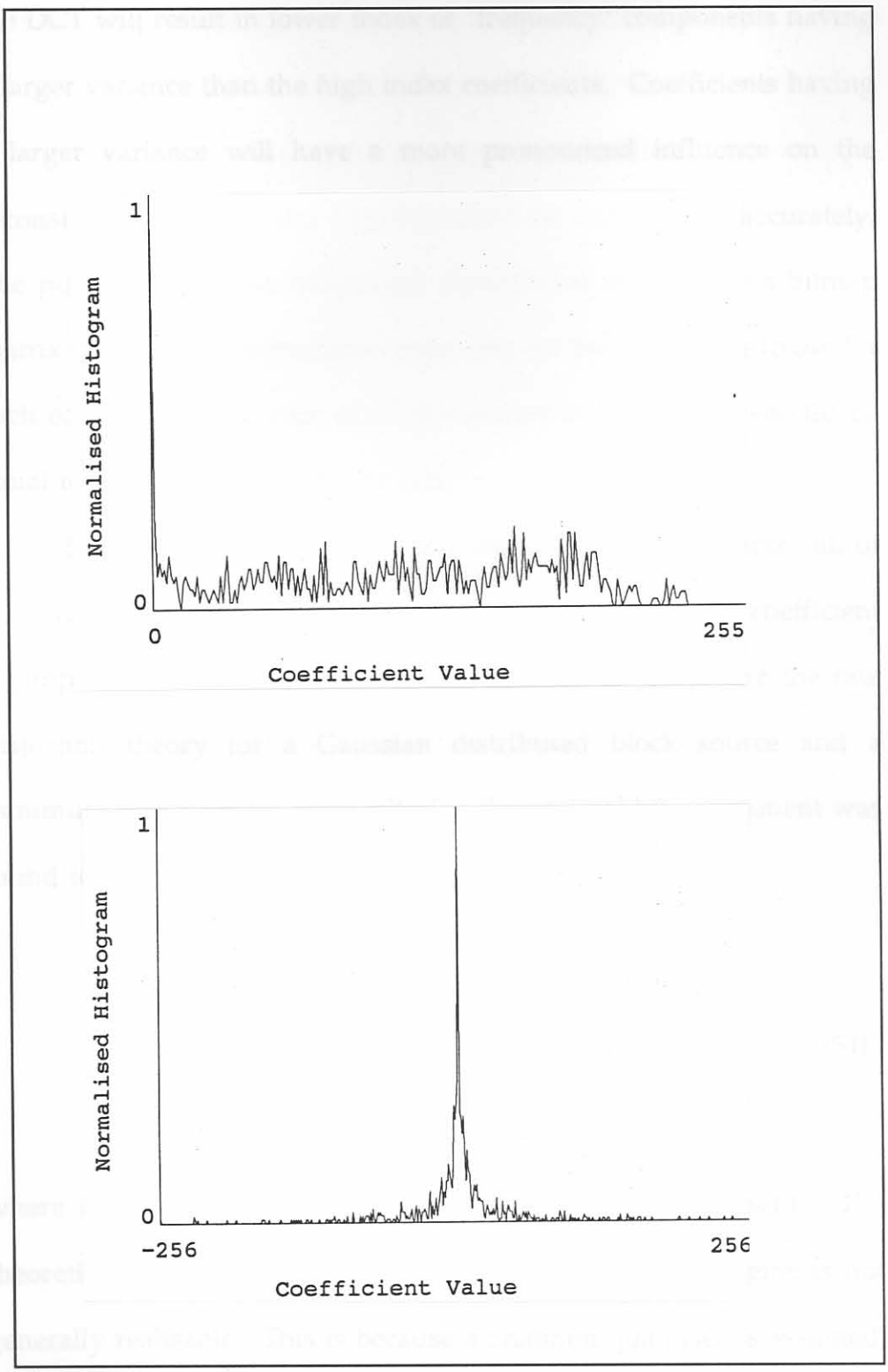

Figure 22 Coefficient distributions for the images GIRL using an 8x8 DCT.

The output of a two dimensional DCT is considered to be a vector under block quantisation. The energy compactation property of

the DCT will result in lower index or "frequency" components having a larger variance than the high index coefficients. Coefficients having a larger variance will have a more pronounced influence on the reconstructed image, and therefore need be coded more accurately. The purpose of the bit assignment algorithm is to generate a bitmap matrix that contains information regarding the number of bits to use for each coefficient. The sum of all the entries in this matrix should be equal to the desired average bit rate.

Several methods exist for computing this bitmap matrix, all of them have in common that the number of bits assigned to a coefficient is proportional to the variance of that coefficient. Applying the rate distortion theory for a Gaussian distributed block source and a minimum mean square error criterion the optimal bit assignment was found to be [1,7],

$$b_i = \theta + \frac{1}{2}\log_2 \frac{\lambda_i}{(\lambda_1 \lambda_2 \cdots \lambda_N)^{1/N}} \qquad (51)$$

where λ_i *is the variance of the i th element,*

θ = *desired average number of bits*

where b_i is the number of bits assigned to the ith element. The theoretical performance of the rate-distortion theoretic scheme is not generally realisable. This is because a Shannon quantiser is assumed, which is difficult to achieve practically [7], and the optimally assigned number of bits is not necessarily integer, and may even be negative.

Rounding to zero or the nearest integer is required, which may offset the optimality of the bit assignment.

Besides the rate distortion theoretic method, there is a computational approach to bit allocation [58]. This approach allocates the total number of available bits to the vector on a bit-by-bit basis using a marginal analysis technique.

The overall average quantisation error for an N-dimensional source is

$$D = E\left[\sum_{i-1}^{N} (x_i - \hat{x}_i)^2\right] \tag{52}$$

where x_i is original element, $\hat{x}_i$ is the reconstructed element

Let *f(n)* be the mean-square quantisation error (msqe) of an n-bit quantiser for a source with unity variance. Then, (52) can be written as

$$D = \sum_{i-1}^{N} \lambda_i f(n_i) \tag{53}$$

where n_i is the number of bits assigned to the ith element of the vector. The bit assignment is initialised by setting all the n_i equal to zero, i.e. a zero bit map matrix. Using the variances of each coefficient a marginal return can be computed for the coefficients. The marginal returns basically determine which coefficient would gain most by assigning another bit to that coefficient's bitmap.

The marginal returns are defined by

$$\Delta_i = \lambda_i [f(n_i) - f(n_i+1)]$$

$$\textit{where } \lambda_i \textit{ is the variance of the } i \textit{ th element,} \qquad (54)$$

$$f(n) \textit{ is the msqe}$$

The bit is allocated to the coefficient that has the largest marginal return. This method is repeated until all the bits has been assigned. The computational approach is superior to the rate-distortion theoretic approach since there is no round-off error in the bit assignment. However, its computational load is much heavier than the other approach. The rate distortion approach further assumes that each element of the vector is Gaussian distributed and that a Shannon quantiser is employed. This is not the case for the coefficients of the DCT transform which is predominantly Laplacian distributed [30]. When using a pdf optimised nonuniform quantiser the error for this quantiser should be used in the bit assignment. A list of the msqe of pdf-optimised nonuniform quantisers for Gaussian, Laplacian, and Gamma distributions is given in Table II [4,58]. It is interesting to note that the differential decrease in error for all distributions tends toward that of the Shannon quantiser, i.e. four, for large n. This means that it might not be necessary to compute the exact error values for large n.

n	f(n)			
	Shannon	Gaussian	Laplacian	Gamma
0	1.0	1.0	1.0	1.0
1	0.25	0.3634	0.5	0.668
2	0.0625	0.1188	0.1963	0.32
3	0.015625	0.03744	0.07175	0.1323
4	0.0039062	0.01154	0.02535	0.0501
5	0.00097656	0.003495	0.008713	0.01784
6	0.00024414	0.001041	0.002913	0.006073
7	0.00006104	0.0003035	0.0009486	0.001996
8	0.00001526	0.00008714	0.0003014	0.0006379

Table II Quantisation Errors of Shannon Quantiser and Max Quantisers for Gaussian, Laplacian, and Gamma Distributions.

F. Adaptive Quantisation

It has been noted in previous discussions that the statistics of real images are spatially variant. The performance of the quantiser could be increased if we could make the quantiser adaptive to local statistics in the image. The main advantage associated with adaptive quantisation is the improvement in the ability of the codec to code detail in the image.

Several methods to achieve this has been presented in the literature [5,7,8,17]. Most of the techniques use some activity measure defined for each block. This activity measure is mostly related to the ac-energy or the variance of the block's coefficients. In the method by Chen [5], the image is classified into four different classes according to

the variance of the blocks. A bitmap matrix is generated for every class. This increases the overhead associated with the quantisation information. It has been estimated by Chen that the overhead is approximately 0.034 bits per class. This places a limit on the number of classes that are practical for adaptive coding.

The purpose of this section is to investigate the relationship between the improvement in image quality and the number of *classes*. In other words the optimal number of classes will be determined using empirical techniques. The classification will consist of computing the ac-energy of each block and dividing the blocks equally between the different classes. To keep the bit assignment optimal, the algorithm assigns bits, using the marginal technique, concurrently to all bitmap matrixes. In other words the bits are spread out between the classes on a largest "error reduction" basis.

The results of the simulation is shown graphically in figure 23. Figures 24 to 27 show the test images coded using one class and eight classes respectively. It is clear from the results achieved that adaptive quantisation based on an activity index improves the quality of the image. Other more advanced techniques that exist but have not been used in simulations are the use of masks in the computation of the block energy. This basically involves generating masks that group certain features of the image, i.e. horizontal, vertical, and diagonal lines [17]. Some techniques use the sensitivity of the HVS to different DCT coefficients to generate the masks [12]. Most of these techniques

require a large number of adaptation of parameters to specific images, making them less useful.

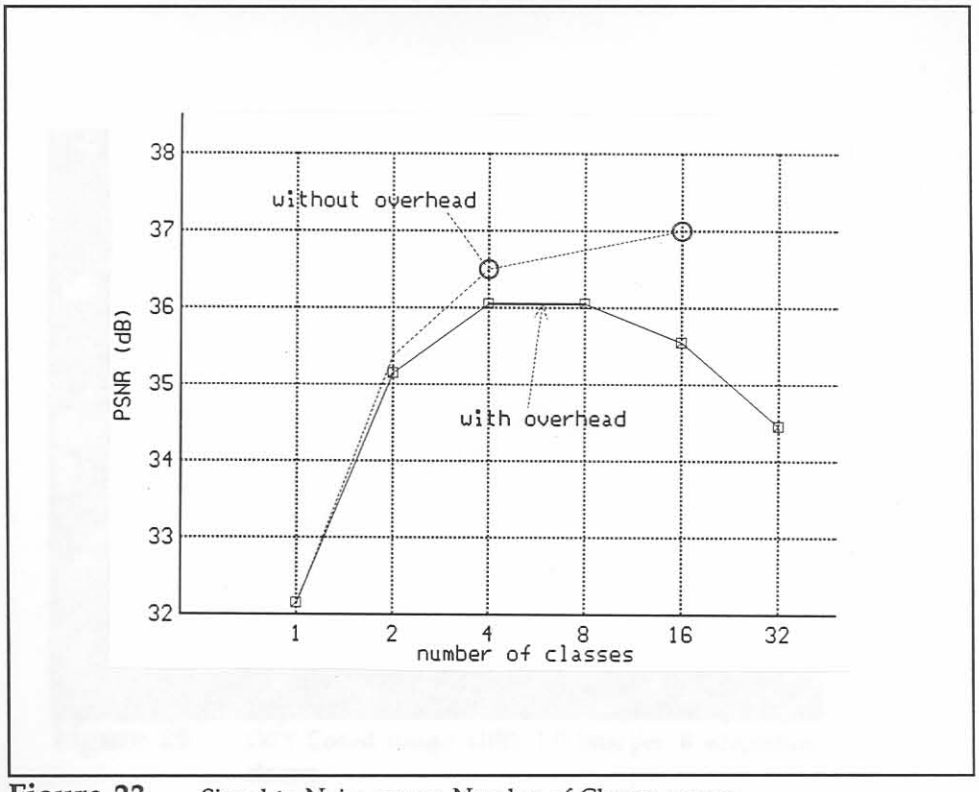

Figure 23 Signal to Noise versus Number of Classes curves

Figure 24 DCT (8x8) Coded Image: GIRL 1.0bits/pel, one adaptation class.

Figure 25 DCT Coded Image: GIRL 1.0 bits/pel. 8 adaptation classes.

Figure 26 DCT Coded Image: ROAD 1.0 bits/pel. 1 Adaptation Class.

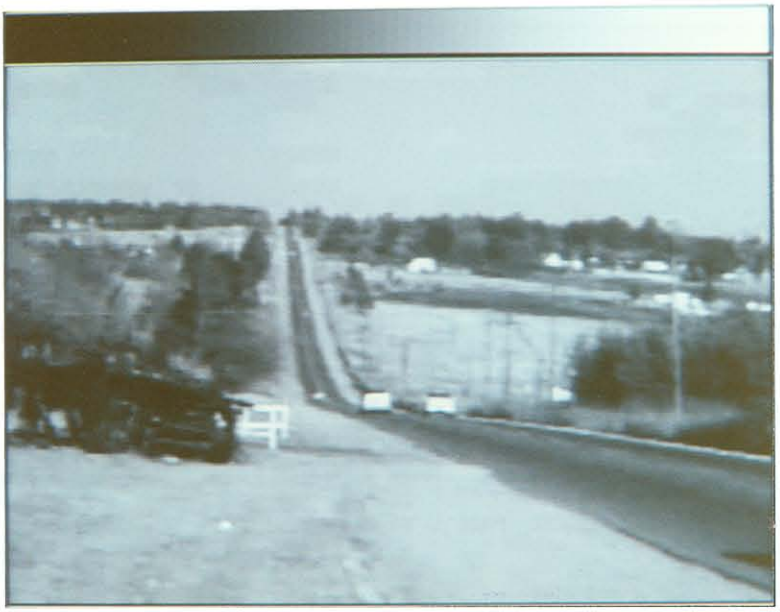

Figure 27 DCT Coded Image: ROAD 1.0 bits/pel. 4 Adaptation Classes.

IX. Reducing the Block-Effect

The block-effect owes its existence to the independent processing of the sub-images, of a segmented image. In the segmentation process the statistical dependencies beyond the border of a block is not taken into account in DCT transform coding. Quantisation of the blocks introduces independent errors among the blocks that causes the discontinuities at the borders between blocks which is observed as the block effect. The block-effect origin is demonstrated graphically in figure 28. The discontinuities are inherent to the basis functions used in the DCT. A graph of the normalised discontinuity at the edges of the DCT is shown in figure 29. It can be seen that the lower "frequency" functions contain large discontinuities and would thus contribute more towards the block-effect.

The energy compactation should be viewed in conjunction with the "discontinuity size" to predict the influence of the quantisation of different coefficients on the block-effect. An experiment was conducted in which the low "frequency" components were first coarsely quantised and then the higher "frequency" components. The results together with the quantisation matrixes are shown in figures 30 to 33. From these results it is clear that quantisation of different coefficients will have different kinds of visual distortion. Low frequency quantisation led to a more pronounced block-effect, while high frequency quantisation led to a more grainy type of distortion.

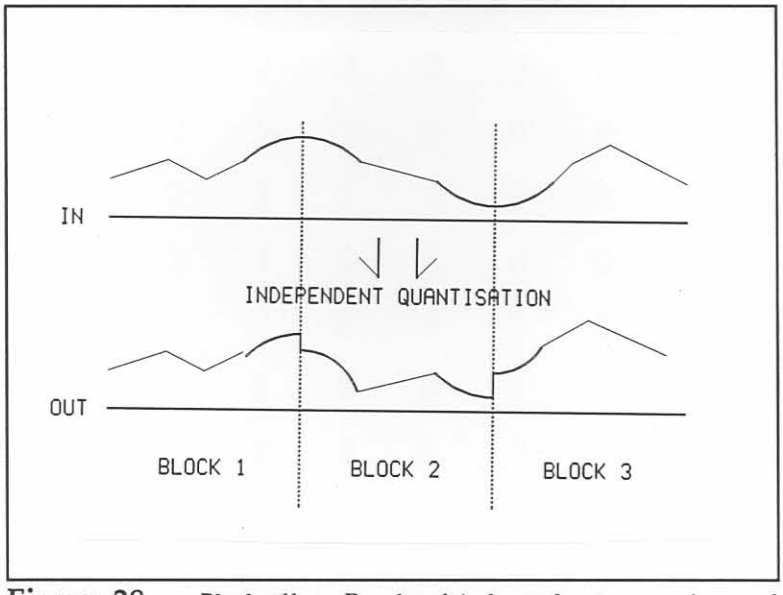

Figure 28 Block-effect: Result of independent processing and quantisation of blocks.

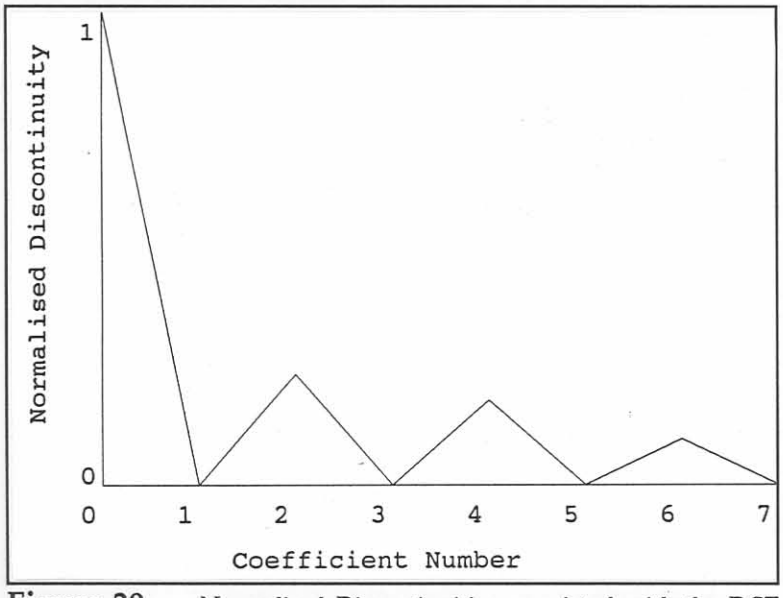

Figure 29 Normalised Discontinuities associated with the DCT Basis Functions.

9	2	2	2	2	8	8	8
2	2	2	2	2	8	8	8
2	2	2	2	8	8	8	8
2	2	2	8	8	8	8	8
2	2	8	8	8	8	8	8
8	8	8	8	8	8	8	8
8	8	8	8	8	8	8	8
8	8	8	8	8	8	8	8

Figure 30 Low frequency bitmap matrix for quantisation experiment.

Figure 31 Low Frequency Quantisation Experiment: GIRL

9	8	8	8	2	2	2	2
8	8	8	8	2	2	2	2
8	8	8	2	2	2	2	2
8	8	2	2	2	2	2	2
2	2	2	2	2	2	2	2
2	2	2	2	2	2	2	2
2	2	2	2	2	2	2	2
2	2	2	2	2	2	2	2

Figure 32 High frequency quantisation experiment- bitmap matrix.

Figure 33 High Frequency DCT Quantisation Experiment: GIRL

The block-effect is a highly visible type of distortion, to a human observer, as a result of the periodic nature thereof and the effect it has on features crossing block-boundaries. At low bit rates the effect becomes very pronounced and may render the transform coder useless.

In this section four techniques will be discussed that attempt to reduce the block-effect. The techniques are filtering, overlapping, using a visual error criterion, and lapped transforms. The first two techniques will only be discussed briefly since they contain inefficiencies in solving the problem. The last two techniques, using the HVS and lapped transforms, each lead to usable improvements in the quality of the reconstructed image. The lapped transforms have been found to decrease the blocking effect considerably as well as resulting in higher coding gains than the corresponding DCT.

A. Filtering

The first and most obvious solution to the problem, is the use of a space variant filter along the boundaries of the blocks, called a post-filter. The post filter performs a smoothing action from one block to the next, with the result that features crossing boundaries tend to be blurred. This blurring can be reduced by using a pre-filter that enhances high frequency detail along the borders of the blocks to offset the low-pass filtering effect of the smoothing filter. Since high frequency detail is enhanced by the pre-filter, the image will require

more bits to quantise to achieve equal fidelity. A nonlinear space-variant postprocessing technique which smooths jagged edges without blurring them, and also smooths out abrupt intensity changes in monotone areas has been proposed by Arch [66]. The disadvantage of filtering methods is that they invariably lead to a reduction in the coding gain. Results from using the spatially variant filter are given in figure 34 and 35. Figure 34 contains the original coded image and figure 35 contains the filtered image. The block-effect seems less but blurring has occurred along the edges of the blocks. The filter that was used simply replaced the border pels with their average value.

Figure 34 DCT coded image: GIRL - block size = 8x8, bit rate = 0.5 bits/pel.

Figure 35 Filtered Image: GIRL

B. Overlapping

A second method is that of overlapping of adjacent blocks, similar to the overlap and add methods used in speech processing. The overlapping of blocks is illustrated in figure 36. This method works well, since it takes the statistical dependencies into account. In the overlapping method, the blocks overlap slightly, so that redundant information is transmitted for samples at the block boundaries. The receiver averages the reconstructed samples from the neighbouring blocks, in the overlapping areas. The disadvantage of this approach is the added redundancy that causes an increase in the bit rate. No results are given in this section since it is similar to that of the LOT, that will be discussed in detail in a following section.

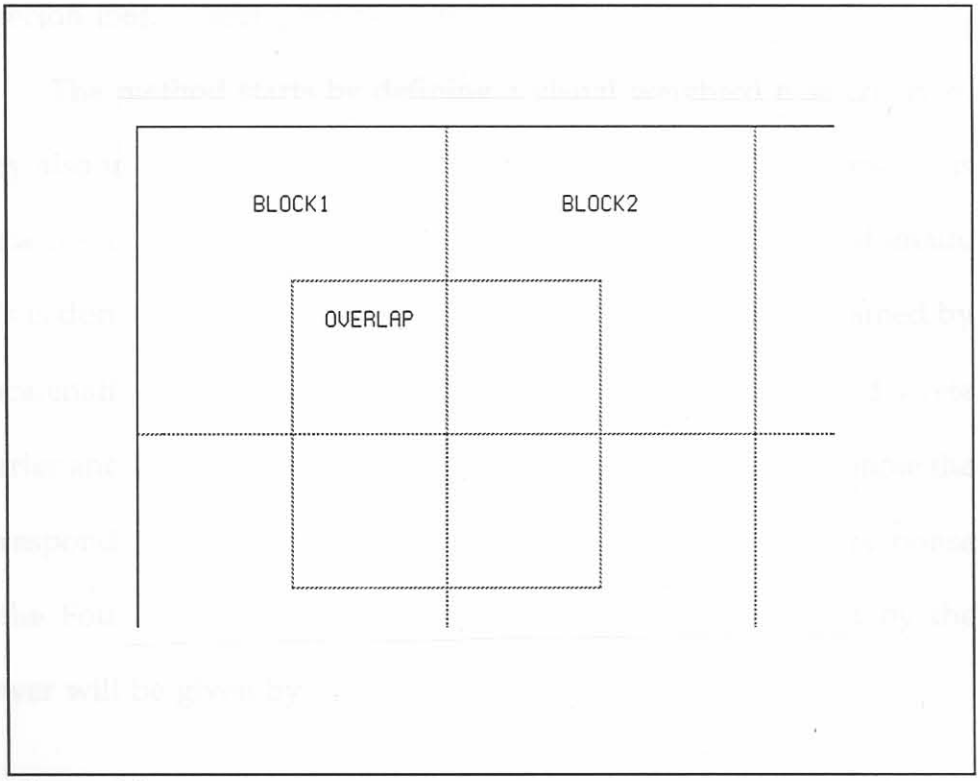

Figure 36 Overlapping of blocks in the transform domain.

C. Visual Error Criterion

A third method for reducing the block-effect is to optimise the bit allocation for quantisation. For example, the use of the human visual system (HVS) in the bit allocation algorithm will result in a more optimal allocation, that takes the user of the information into account. Using the HVS allows one to minimise the visual error, rather than the mean square error (mse) criterium normally used. This means that the visibility of the errors, such as the block-effect, will be taken into account when the coefficients of the transform are quantised. What needs to be done to implement this technique is to determine a HVS weighing matrix that determines the relative importance of the different coefficients. A method that achieves this has been introduced by Eggerton [56].

The method starts by defining a visual weighted mse criterion. They also use the HVS model by Mannos [16], but since that model is in the frequency domain it has to be transformed to the DCT domain. This is done as follows: Let x be a one dimensional vector obtained by concatenating the image rows. Let F and C represent the discrete Fourier and the discrete Cosine transforms and let X_F and X_C denote the corresponding vector of transforms. If H represents the HVS response in the Fourier domain, the DFT of the image as perceived by the viewer will be given by

$$Y_F = HX_F = HFx \tag{55}$$

The corresponding spatial function is

$$y_F = F^{-1}HFx \tag{56}$$

so that the DCT equivalent of the response Y_F will be

$$\begin{aligned} Y_C &= Cy_F = CF^{-1}HFx \\ &= CF^{-1}H(CF^{-1})^{-1}Cx \\ &= AHA^{-1}X_C \end{aligned} \tag{57}$$

$$\textit{where} \quad A = CF^{-1}$$

If X_C is set to a constant value, the elements of Y_C provide the relative importance of the DCT coefficients to the human observer.

The first application of this result, using a 16x16 DCT and 16x16 DFT, gave a weighing matrix that actually worsened the block-effect. This was because the discontinuities at the block edges were not taken into account. The contrast inside a block appeared to be sharper than that of the normal mse codec, however the block effect made the technique useless. A method that took the block effect into account was given by Eggerton [56], in which the DCT is done on a block, say 16x16, and the DFT on the whole image. A flow diagram of this method is given in figure 37. The weighing matrix obtained for a block size of 8x8 is shown in figure 38, and in figure 39 the image Girl coded to 1.0 bits. It was found that the weighting matrix has little effect on image quality for rates above one bit per pel.

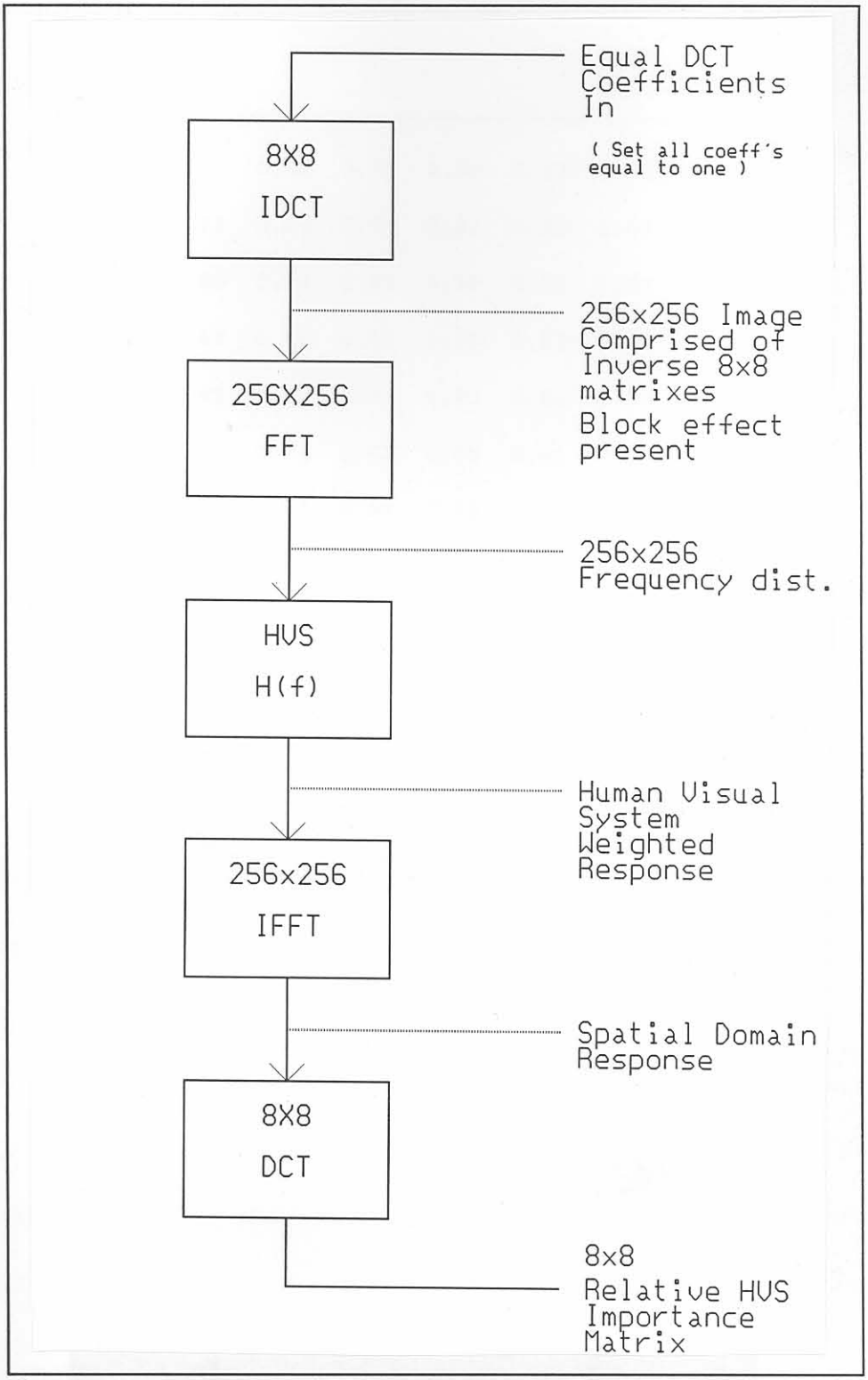

Figure 37 Processing steps to obtain the DCT domain weighting matrix from the Fourier domain function, while keeping the block boundary changes in mind.

0.05	0.85	0.82	0.89	1.00	0.77	0.90	0.61
0.84	0.71	0.86	0.67	0.81	0.58	0.69	0.47
0.82	0.86	0.94	0.85	0.99	0.73	0.87	0.59
0.89	0.67	0.85	0.62	0.76	0.53	0.64	0.43
1.00	0.82	1.00	0.77	0.92	0.65	0.79	0.52
0.78	0.58	0.74	0.53	0.65	0.45	0.54	0.37
0.90	0.69	0.87	0.64	0.79	0.54	0.66	0.44
0.61	0.47	0.59	0.43	0.53	0.37	0.44	0.30

Figure 38 Weighing matrix for 8x8 DCT with maximum display frequency of 6 cycles/degree.

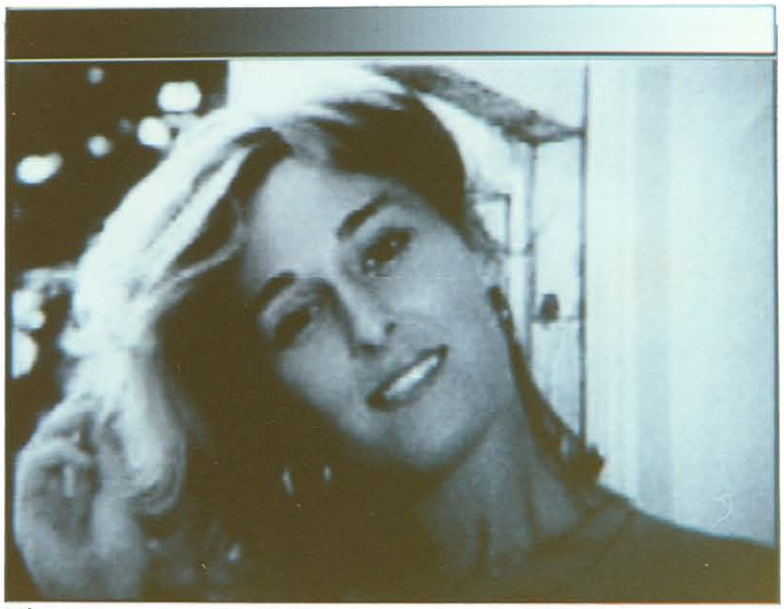

Figure 39 Human Visual System weighed DCT coded image GIRL, 1.0 bits/pel.

D. Lapped Transforms

The first of these transforms called the lapped orthogonal transform (LOT), was introduced by Cassereau [61]. Subsequently, Malvar and Staelin [62] introduced a new algorithm for generating LOT, that used the DCT as basis. By using the DCT as basis for the LOT, this algorithm is very attractive for practical implementation since it can use existing DCT algorithms and chips. Cassereau in conjunction with Staelin and de Jager recently published another paper [61], wherein an augmented Lagrangian method has been used to derive the LOT basis functions. Recognising the LOT as a special case of perfect reconstruction filter banks, Malvar [63] gave a new version of the lapped orthogonal transform, which can be efficiently computed for any transform length. He also introduced the modulated lapped transform (MLT), which is based on a modulated quadrature mirror filter (QMF). He found that the MLT can be efficiently computed by means of a type-IV discrete sine transform.

Malvar [63] found that the LOT and MLT are both asymptotically optimal lapped transforms for coding an AR(1) process with high inter-sample correlation. The coding gains of the LOT and the MLT are higher than that of the DCT for similar size, and were found to be close to that of a DCT of twice the size.

The DCT based LOT has been chosen for the simulations, based on the advantages of using the DCT as is, as well as the numerical stability of the LOT basis function when derived from the DCT. The derivation for the optimal LOT is given in Appendix A. The final form of the optimal LOT was found to be

$$P_o = \frac{1}{2}\begin{bmatrix} D_e - D_o & D_e - D_o \\ J(D_e - D_o) & -J(D_e - D_o) \end{bmatrix}\begin{bmatrix} I & 0 \\ 0 & Z \end{bmatrix} \tag{58}$$

where D_e is the even cosine basis functions, D_o is the odd cosine basis functions, J is the counter identity matrix, and Z is the optimising matrix. The fast implementation of the LOT is also given in Appendix A. A brief summary of the characteristics of the LOT is given:

1. The LOT requires approximately 30%-100% more computations than DCT, if the DCT is integrated into the algorithm,
2. The LOT is asymptotically optimal for first order Markov processes as the correlation coefficient approaches unity,
3. The LOT can be optimised to the statistics of the image by choosing the correlation coefficient and using it in the computation of the optimisation matrix,

4. The LOT decreases the block effect considerably as a result of the overlapping nature of its basis functions, and that they decay smoothly towards zero,
5. The LOT has a higher coding gain (0.3dB) than a DCT of the same size.

To compare the results achieved with the LOT to those of the DCT the test images were coded using the simple non-adaptive algorithm with Lloyd-Max quantisation for bit rates 2.0, 1.5, 1.0, and 0.5 bits/pel. The LOT fared better in most cases with a significant reduction in the block-effect. The block-effect was still visible at the lower bit rates but was less than that of the DCT. Graphical results are plotted in figure 40 and pictures for 1.0 and 0.5 bits/pel are shown for comparison purposes in figures 41-44. From figure 40 it can be seen that the LOT achieved a better signal to noise ratio than the DCT. This improvement was in accordance with what was expected.

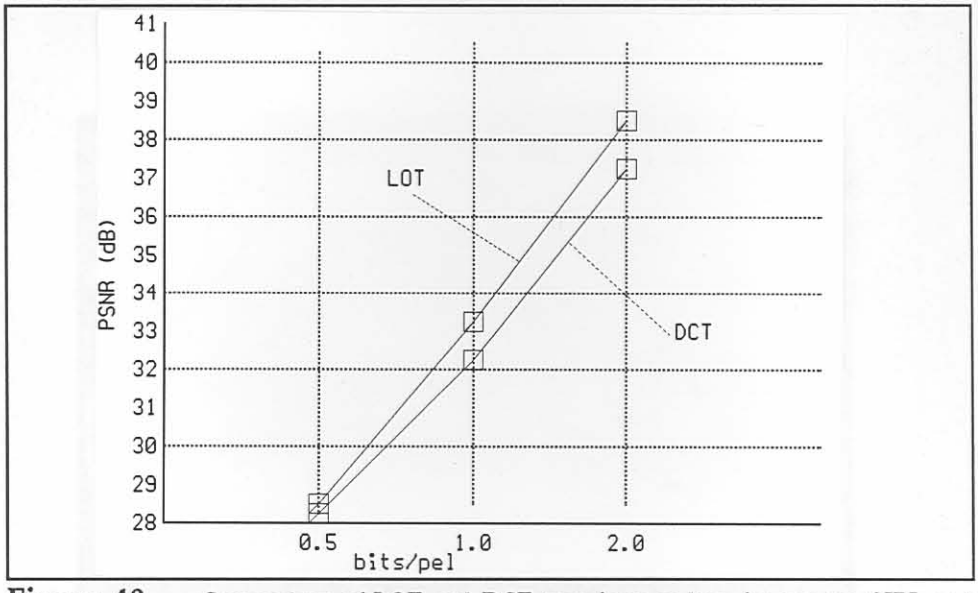

Figure 40 Comparison of LOT and DCT transform coding for images GIRL and ROAD

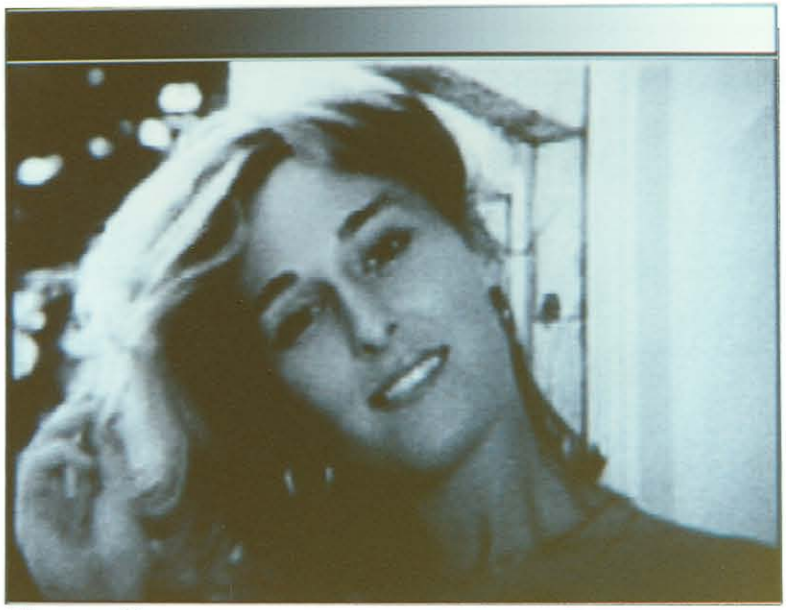

Figure 41 DCT Coded Image: GIRL - 1.0 bit/pel, 8x8 block size.

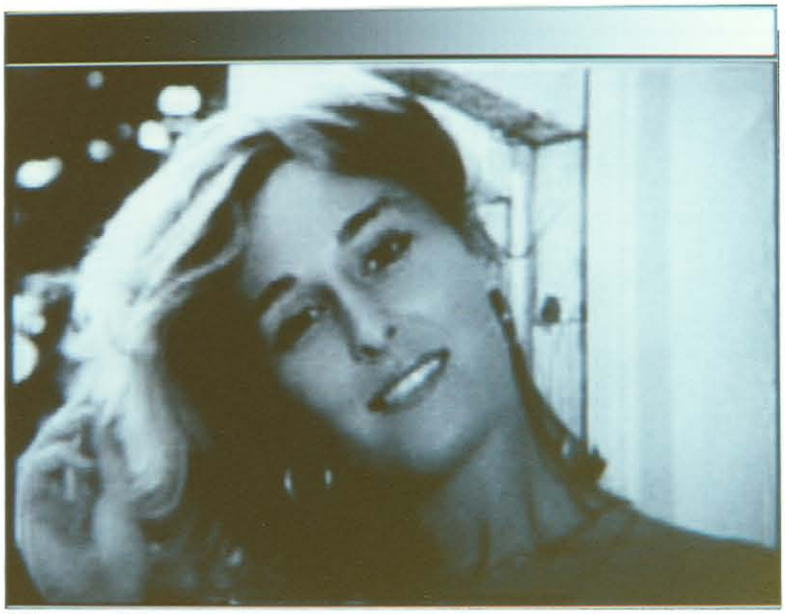

Figure 42 LOT coded Image: GIRL - 1.0 bit/pel, 8x8 block size.

Figure 43 DCT Coded Image: ROAD 0.5 bit/pixel, 8x8 block size.

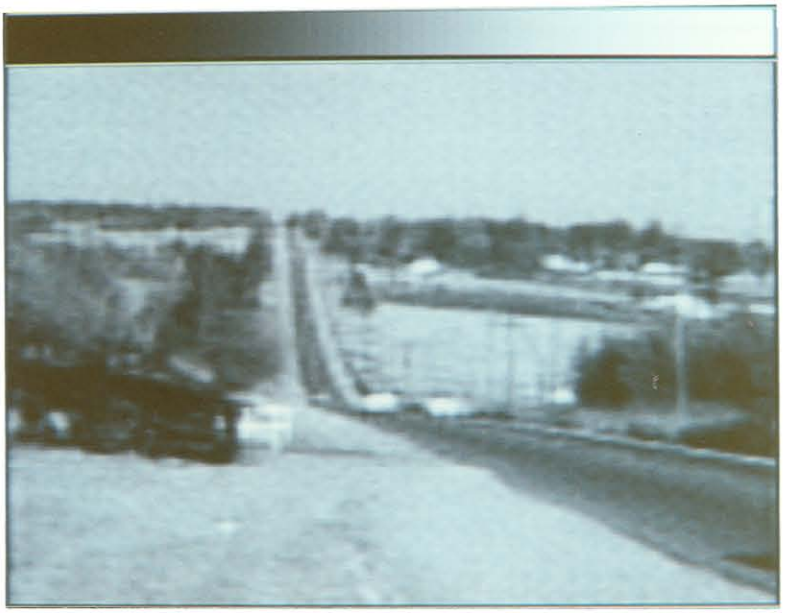

Figure 44 LOT Coded Image: ROAD 0.5 bits/pel, 8x8 Block size.

X. Combined Algorithm

In this section the results from the other sections will be integrated into one algorithm. The algorithm basically consists of a visually-adaptive lapped-transform encoder with optimised quantisation. The transform section will consist of a LOT transform for reducing the block-effect. The quantisation step will consist of a uniform quantiser followed by source coding, since this type of coding took better advantage of correlation between coefficients and blocks. The HVS is introduced in the determination of the step size of the uniform quantiser. The structure of the final algorithm is shown in figure 45.

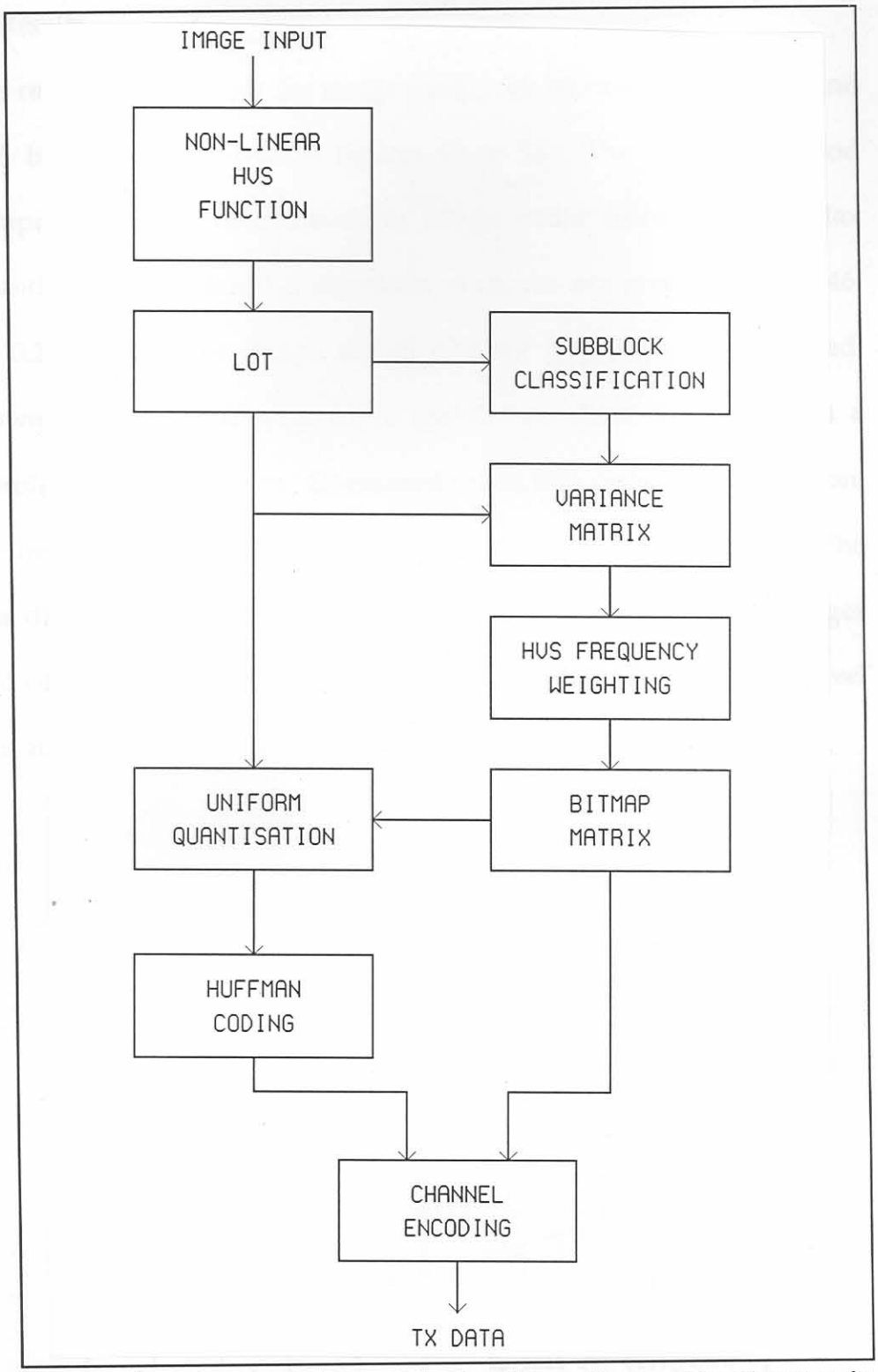

Figure 45 Structure of image codec for high quality encoding of images for transmission.

A. Results

The results achieved for the image codec, for bit rates between 2.0 and 0.25 bits/pel, is shown in figures 47 to 58. The results are good compared to the basic transform image codec using a Lloyd-Max quantiser. A numerical comparison of results are given in figure 46. At 0.25 bits/pel the image lacked contrast and were a bit blurred. However, the results were more useful than those achieved with a simple DCT based codec. Compared to the rate distortion simulation, the images coded to 1.0 and 0.5 bits performed slightly inferior. The rate distorted images appeared slightly sharper than the coded images and contained less artifacts. The block-effect was reduced up to a level that it only became visible for low bit rates.

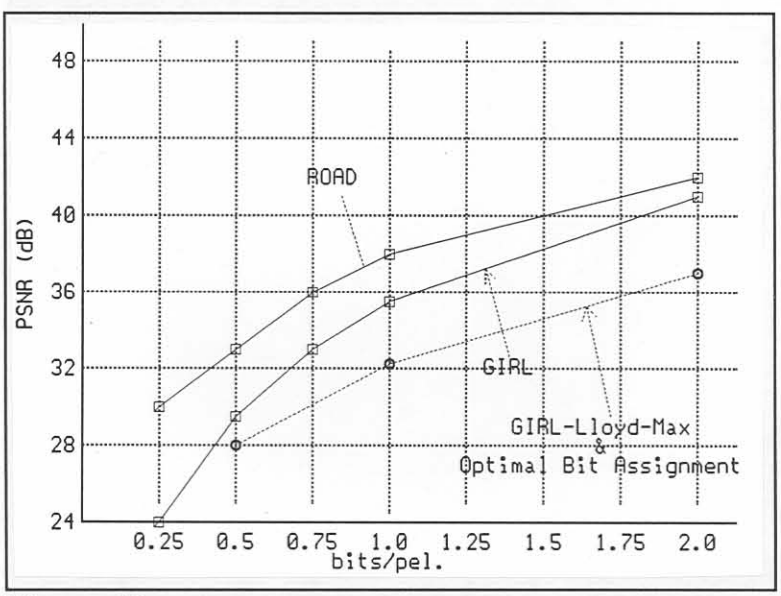

Figure 46 Numerical Results for Images Coded with the Combined Algorithm.

Figure 47 Original Image: GIRL (256x256x8)

Figure 48 LOT Coded Image: GIRL 2.0 bits/pel.

Figure 49 LOT Coded Image: GIRL 1.0 bits/pel.

Figure 50 LOT Coded Image: GIRL 0.75 bit/pel.

Figure 51 LOT Coded Image: GIRL 0.5 bit/pel.

Figure 52 LOT Coded Image: GIRL 0.25 bits/pel.

Figure 53 Original Image: ROAD (256x256x8)

Figure 54 LOT Coded Image: ROAD 2.0 bits/pel.

Figure 55 LOT Coded Image: ROAD 1.0 bits/pel.

Figure 56 LOT Coded Image: ROAD 0.75 bits/pel.

Figure 57 LOT Coded Image: ROAD 0.5 bits/pel.

Figure 58 LOT Coded Image: ROAD 0.25 bits/pel.

B. Channel Error Simulation

For the channel error simulation random errors were made in the coefficients of the coded data. For the experiments the bit rate was chosen to be 1 bit/pel. Errors in the quantisation information are considered critical, thus it is assumed that this information will be sufficiently protected with an error correction scheme. For a picture coded to one bit per pixel the total number of bits is 65536, which makes simulation of channel errors difficult for error probability less than 10^{-5}. The influence of errors in the range 10^{-5} to 10^{-3} was investigated on images coded with both the DCT and the LOT. Results are shown graphically in figure 59 and images for error probability of 10^{-4} are shown in figures 60 to 61. The results show that the LOT is superior in its ability to compensate for channel errors, since each block is reconstructed from the overlapping of four blocks.

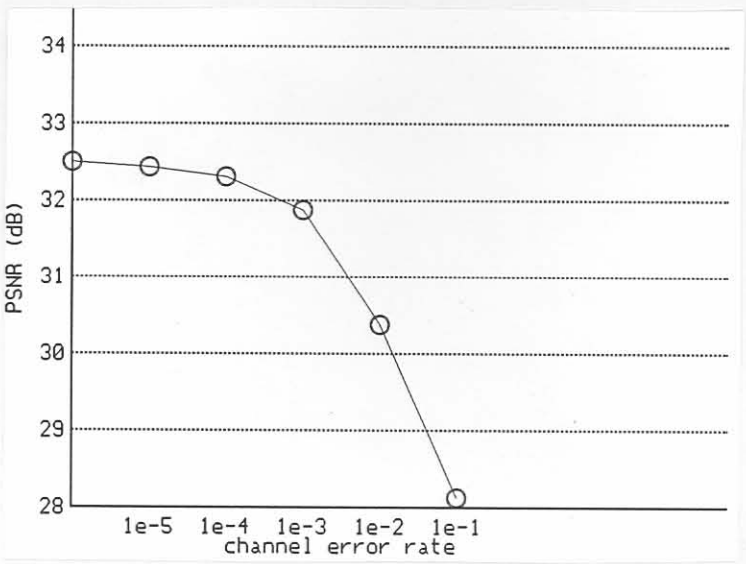

Figure 59 Signal to Noise Ratios for different channel error rates.

Figure 60 DCT (8x8) Coded Image: GIRL @ 1.0 bits/pel, 10^{-4} Error probability.

Figure 61 LOT Coded Image: GIRL 1.0 bits/pel, 8x8 block size, 10^{-4} Probability of Error.

XI. Conclusion

The thesis started by stating the information theory guidelines for image coding. Next the image spatial statistics was investigated and the Markov image model was presented. The thesis continued with a discussion of the human visual system and its application in transform image coding. The use of the rate distortion theory was also presented in this section. The next step was to define the quality criteria that were used to measure the codec's performance.

The basic transform coder structure was given and the different subsections were discussed. In this discussion the use of the DCT, as choice of transform, was substantiated. The different sources of errors in the basic transform coder structure were inspected and presented. The quantisation of the coefficients was investigated next. Three models for quantisation were presented, the compander, the Lloyd-Max quantiser, and the uniform quantiser followed by source coding. The last method outperformed the others as a result of its ability to adjust to the specific statistics of the coefficients as well as an ability to take advantage of inter-block as well as inter-coefficient correlations.

Next the optimal assignment of bits to the different coefficients were presented. It was shown that the marginal analysis bit assignment provides better results than the rate distortion theoretic approach (RDTA), as a result of several shortcomings of the RDTA.

The bit assignment was then made spatially adaptive, i.e. the image was classified into different regions of similar statistics. This improved the coding of detail in the images, especially when a Lloyd-Max quantiser was used, and to a lesser extend when source coding was used.

The focus then moved to the elimination of the block-effect, and four methods were presented that attempted to reduce the blocking effect. These included filtering, overlap and add method, visual error minimisation, and lapped orthogonal transforms (LOT). Of these the LOT was found to be the most successful in reducing the block-effect while at the same time increasing the coding gain.

The best results of each section were then integrated to form the final algorithm. This algorithm was tested for bit rates between 2.0 and 0.25 bits/pixel. Good results were achieved throughout the rate range with 2.0 bits/pel virtually indistinguishable from the original and 0.25 bits/pixel very usable. The algorithm was then tested for sensitivity to channel errors for error probability between 10^{-3} and 10^{-5}. Here, it was seen that the overlapping nature of the LOT is desirable for image reconstruction in the presence of channel errors.

It was found that the final algorithm performed close to that of the rate distortion simulation with some improvement still possible. The improvement could possibly be achieved by further improvements in the coefficient quantisation. These improvements could take the form of direction adaptive masks, to better group blocks of similar statistics.

Appendix A: Derivation of the LOT

The derivation of the LOT by Malvar [62], and Cassereau et al. [61], is quite similar, except for the actual derivation of the basis functions. The derivation given here is basically that of Malvar [62], but with comments from [61], Malvar [63], and Le Gall [47] for further clarification.

Basic Properties of the LOT

To take the statistical interdependence of adjacent blocks into account, the transform needs to allow for the overlapping of basis functions between blocks. The length L, of the basis functions, must therefore be greater than that of the subblock size N, i.e. L>N. To avoid an increase in data rate the number of transform coefficients must be kept equal to the block size, which is the major difference between this technique and that of overlap- and add techniques.

The LOT is defined as a separable unitary transform for which the basis functions corresponding to adjacent data blocks overlap in the image domain [61].

Thus the LOT transform, for a segment consisting of M blocks of size N, can be numerically defined by [62]

$$T = \begin{bmatrix} P_1 & & & 0 \\ & P_0 & & \\ & & \ddots & \\ & & & P_0 \\ 0 & & & P_2 \end{bmatrix} \tag{1}$$

P_0 is an LxN matrix that contains the LOT basis functions for each block. The matrices P_1 and P_2 are introduced because the first and last blocks of a segment have only one neighbouring block, and thus the LOT for the first and last blocks needs to be defined in a slightly different way to compensate for boundaries.

The LOT of a single block is not invertible, since the matrix P_0 is not square. Nevertheless, in terms of reconstruction of the complete sequence, all that is required, is that the transform T, of the complete sequence be invertible. Orthogonality of T is also a desirable property, since it guarantees good numerical stability, and is also necessary for good energy compactation. In order for T to be orthogonal, the columns of P_0 must be orthogonal,

$$P_0^t P_0 = I\ , \tag{2}$$

With this condition satisfied, the transform process yields a non-redundant representation of the digitised image. The next condition for the orthogonality of T, requires that the overlapping basis functions of neighbouring blocks must also be orthogonal,

$$P_o^t W P_o = P_o^t W^t P_o = 0 \tag{3}$$

where I is the identity matrix, and the shift operator W is defined by

$$W = \begin{bmatrix} 0 & I \\ 0 & 0 \end{bmatrix} \tag{4}$$

The shift operator simulates the overlapping of basis functions from adjacent blocks. The identity matrix in (4) is of order L-N.

For image coding it is important that the transform exhibit good energy compactation properties. The optimal transform, given second order statistics, is the Karhunen Loeve transform. Using this fact, and the modelling of the image as a first order Gauss-Markov process, it was found that the DCT is asymptotically equivalent to the KLT for correlation factors close to one. The 2NX2N correlation matrix is defined as

$$R_{xx} = \rho^{|k-l|} \qquad k, l = 1,2,\ldots,L \tag{5}$$

where ρ *is the correlation coefficient.*

Since R_{xx} is symmetric and Toeplitz, its eigenvectors (which define the KLT) are either symmetric or antisymmetric [62], i.e.,

$$R_{xx}\, y = \lambda\, y \;\Rightarrow\; J\, y = y \quad or \quad J\, y = -y \tag{6}$$

where J is the "counter-identity"

$$J = \begin{bmatrix} 0 & \cdots & 0 & 1 \\ 0 & \cdots & 1 & 0 \\ \vdots & & \vdots & \vdots \\ \vdots & & \vdots & \vdots \\ \vdots & & \vdots & \vdots \\ 0 & 1 & & 0 \\ 1 & 0 & \cdots & 0 \end{bmatrix} \tag{7}$$

For the first order Markov process the basis functions of the KLT, consists of an equal number of symmetric and antisymmetric basis functions. From this point of view Malvar [62], decided that a "good" LOT matrix, should comprise of half odd and half even basis functions. To advocate the use of the DCT, Malvar noted that the DCT also has this even-odd symmetry.

The last point given for the use of the DCT, is that the basis functions of the LOT should be as smooth as possible, i.e. sampled sinusoid. The reason for the required smoothness is given, for energy compactation by Malvar [62], and because the mse by itself is not a sufficient goodness criteria for the evaluation of image coding techniques by Le Gall [47]. Intuitively, any discontinuities in the basis functions would give rise to blocking effects. The KLT, for first order Markov processes,

and the DCT are members of the sinusoidal family of unitary transforms [45].

The transform length in [61] and [62] is chosen L=2N for the reason that shorter lengths may cause discontinuities at two positions, rather than at one, and also for convenience in introducing the DCT based LOT. A further desirable property of the LOT is that it should be able to represent the DC value of a flat field with only one coefficient. This can only be achieved if the overlapped lowest basis function has a constant DC value. If L is chosen any other value than multiples of N, discontinuities will be introduced into this basis function which is undesirable. Although L could be any multiple of N, to minimise boundaries, an overlap of two is chosen to minimise processing requirements.

The properties of the desired LOT matrix P_0 are, equal even and odd basis functions, basis functions which are smooth and decay toward zero at the boundaries, and an overlapping of N samples. The shifted orthogonality in (3) forces the decay toward zero of the basis functions.

Optimal LOT in terms of Energy Compactation

The optimal LOT is that transform which maximises the Energy Compactation, since this minimises the bit rate. Assuming that the Markov model is applicable, the energy compactation measure normally used is given by the transform coding gain

Instead of using an iterative technique that searches for the maximum

$$G_{TC} = \frac{\frac{1}{N}\sum_{i-1}^{N}\sigma_i^2}{\left(\prod_{i-1}^{N}\sigma_i^2\right)^{\frac{1}{N}}} \tag{8}$$

where σ_i^2 *is the variance from the autocorrelation matrix,*

$$R_0 = P_0^t R_{xx} P_0 . \tag{9}$$

coding gain as in the technique by Casserau [61], Malvar [62] uses a direct method that, although less sensitive to numerical errors, is less likely to converge to a local minima than that of Casserau. The optimal P_0, as generated by Casserau's method, may not be easily factorable so that a fast algorithm may not exist. The lack of a fast algorithm and sensitivity to numerical errors of Casserau's method made the method of Malvar a better choice. However, it is important to note that Malvar's method doesn't give a *global* optimal LOT, since his approach leads to an optimal LOT that is tied to the choice of P. The choice of P given by Malvar seems to be good since they achieved a slightly higher coding gain than Casserau [62].

Malvar starts by defining a feasible LOT matrix P that may not be optimal. This matrix is then optimised to fulfil the desired features of an optimal LOT as discussed. The optimisation is done by modifying the P matrix with an optimising matrix Z, such that

$$P_0 = PZ \tag{10}$$

is an optimal LOT matrix. P_0 is a feasible LOT matrix for any

orthogonal Z, since it still conforms to the orthogonality definitions in (2) and (3), i.e.

$$P_0^t P_0 = Z^t P^t P Z = Z^t Z = I \tag{11}$$

and

$$P_0^t W P_0 = Z^t P^t W P Z = 0 \tag{12}$$

To compute the Z that will optimise P_0 the transform domain correlation matrix is computed, i.e. substitute (10) into (9)

$$R_0 = Z^t P^t R_{xx} P Z \tag{13}$$

where R_{xx} is the correlation matrix for the first order Markovian process, defined in (7). With R_{xx} and P fixed the coding gain G_{TC} will be maximised when R_o is diagonal, i.e. when Z are the eigenvectors of $P_t R_{xx} P$. Given such a Z the LOT matrix P_0 is optimal.

Malvar [62] defined the feasible LOT as

$$P = \frac{1}{2}\begin{bmatrix} D_e - D_o & D_e - D_o \\ J(D_e - D_o) & -J(D_e - D_o) \end{bmatrix} \tag{14}$$

where D_e and D_o are the NxN/2 matrixes containing the even and odd DCT functions, defined by

$$[D_e]_{nk} = c(k)\sqrt{\frac{2}{N}}\cos\left(\frac{\pi}{N}2k\left(n+\frac{1}{2}\right)\right) \tag{15}$$

and

$$[D_o]_{nk} = \sqrt{\frac{2}{N}}\cos\left(\frac{\pi}{N}(2k+1)\left(n+\frac{1}{2}\right)\right)$$

$$for\ n=0,1,\ldots,N-1,\ k=0,1,\ldots,N/2-1, \tag{16}$$

$$where\ \ c(k) = \begin{cases} 1/\sqrt{2}, & k=0 \\ 1, & otherwise. \end{cases}$$

The basis functions of the feasible LOT P, for a Markov model with a correlation coefficient of 0.95 and n=8, are shown in figure A1, and that of the optimised LOT P_0 in figure A2. Notice the discontinuities in the odd basis functions of the non-optimised LOT.

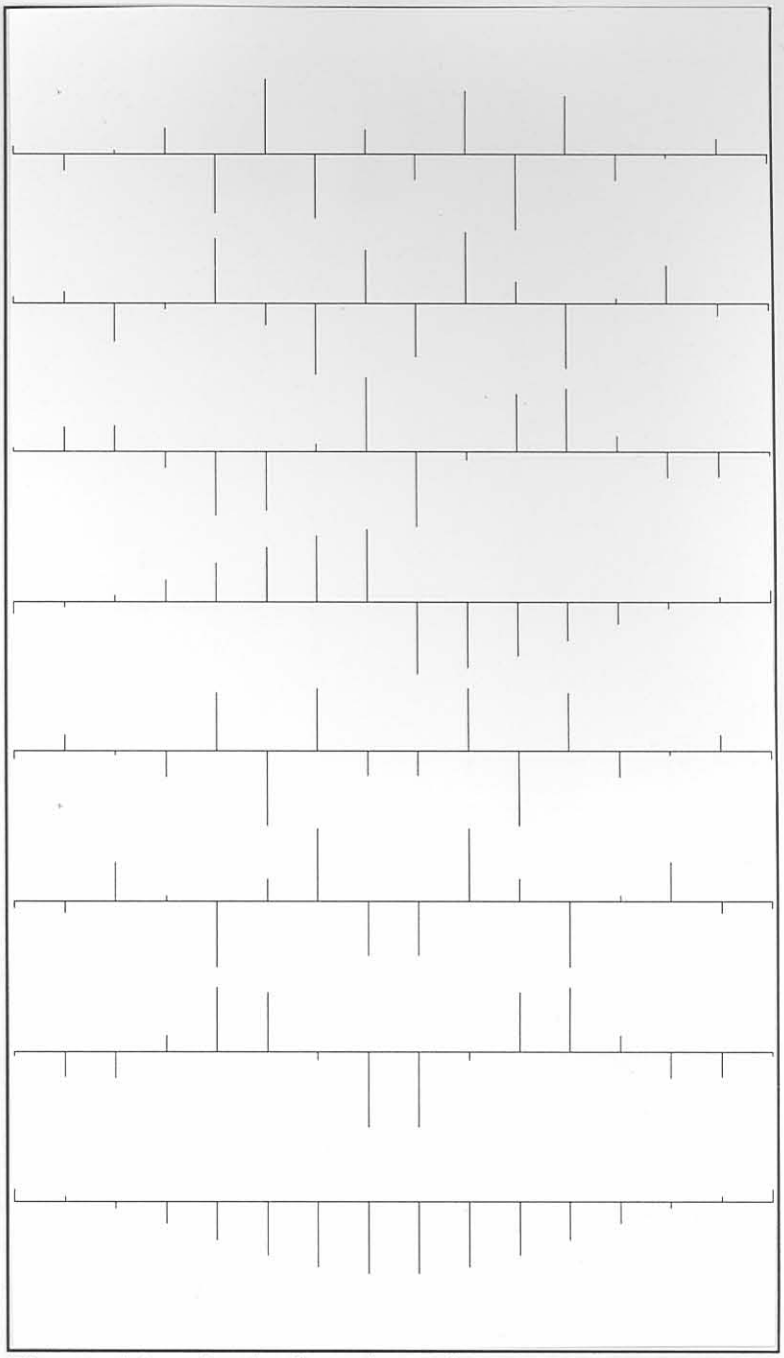

Figure A1 Basis functions for the non-optimised LOT for n=8.

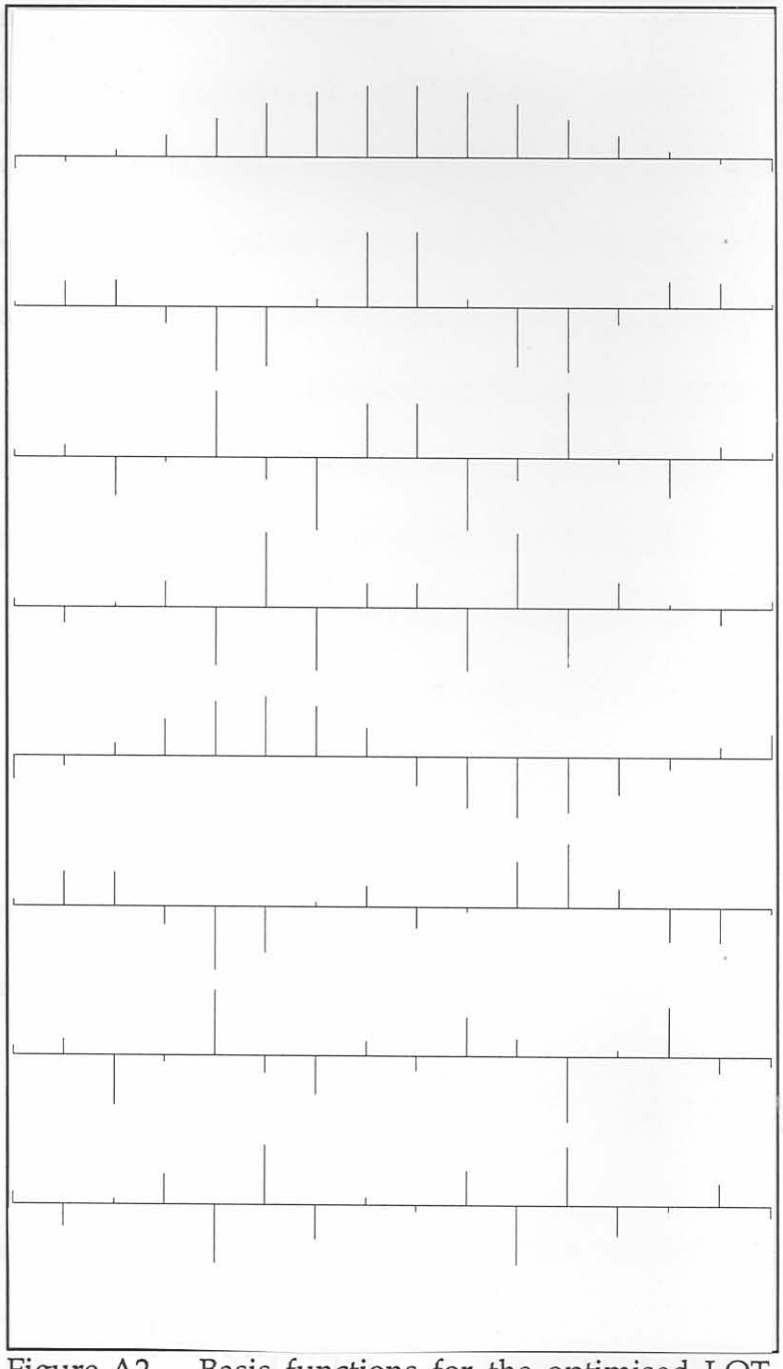

Figure A2 Basis functions for the optimised LOT, correlation coefficient = 0.95, n=8.

The optimising matrix Z may not be factorable in Nlog(N) butterfly stages. However, Malvar introduced two different methods to approximate this matrix for fast implementations. In the first approach the eigenvalue matrix is approximated by a number of matrix rotations. This technique is approximately 30% more computationally intensive than the DCT by itself, but the approximation only keeps for N smaller or equal to 16. The second method based on a sine/cosine transform approximation is valid for larger sizes of N, but is 100% more computationally intensive. The next section describes the two approximations.

Fast Algorithm

A brief summary of the approximation algorithms is given in this section. In both cases the optimising Z can be approximated by

$$Z = \begin{bmatrix} I & 0 \\ 0 & B \end{bmatrix} \tag{17}$$

For the first approximation B is a cascade of N/2-1 plane rotations,

$$B = A_1 A_2 \ldots A_{M/2-1} \tag{18}$$

the plane rotations is defined by

$$A_i = \begin{bmatrix} I^{i-1} & & 0 \\ & Y(\theta_i) & \\ 0 & & I^{\frac{N}{2}-2-(i-1)} \end{bmatrix} \tag{19}$$

$$Y(\theta_i) = \begin{bmatrix} \cos\theta_i & \sin\theta_i \\ -\sin\theta_i & \cos\theta_i \end{bmatrix} \tag{20}$$

where θ_i is the rotation angle.

where I^j is an identity matrix of order j. The rotation angles has been computed by Malvar [62] for n=8 and n=16 and are given in Table A1.

Rotation-angle / π	1	2	3	4	5	6	7
n=8	0.13	0.16	0.13				
n=16	0.42	0.53	0.5	0.44	0.35	0.23	0.11

Table A1 Rotation angles for fast LOT, correlation coefficient = 0.95

The loss in coding gain due to the approximation were computed to be 0.08 dB. The gain over the DCT for this algorithm was 0.32dB for the Markov process.

The approximation to B for any length given by Malvar [63],

$$B = C^{II}_{N/2} S^{IV}_{N/2} \tag{21}$$

where C and S are the DCT type II and DST type IV matrixes, defined by

$$[C^{II}_K]_{kr} = c(k)\sqrt{\frac{2}{K}} \cos\left(\frac{\pi}{K}k\left(r+\frac{1}{2}\right)\right) \tag{22}$$

with c(k) as in (15), and

$$[S^{IV}_K]_{kr} = \sqrt{\frac{2}{K}} \sin\left(\frac{\pi}{K}\left(k+\frac{1}{2}\right)\left(r+\frac{1}{2}\right)\right) \tag{23}$$

The LOT basis functions generated with this approximation satisfies the following symmetry condition:

$$[P_o]_{nk} = (-1)^k [P_o]_{2n-1-n,k} \tag{24}$$

which guarantees that all the filters in the analysis and synthesis filter banks have linear phase, which is an advantageous property for subband coding.

The P_0 matrix can be restuctured to isolate the DCT section from the LOT modification and optimation sections, i.e.

$$P_o = \frac{1}{2}\begin{bmatrix} D_e & D_o & 0 & 0 \\ 0 & 0 & D_e & D_o \end{bmatrix} \begin{bmatrix} I & I & 0 & 0 \\ I & -I & 0 & 0 \\ 0 & 0 & I & I \\ 0 & 0 & I & -I \end{bmatrix} \begin{bmatrix} 0 & 0 \\ I & I \\ I & -I \\ 0 & 0 \end{bmatrix} \begin{bmatrix} I & 0 \\ 0 & B \end{bmatrix} \tag{25}$$

Most of the operations after the DCT consists of additions and

subtractions, as can be seen from the matrix contents of (25). Only one DCT need to be computed per LOT as can be seen in the flowgraph shown in figure A3. P_1 and P_2 is computed by reflecting the data at the boundaries. This concludes the derivation of the LOT algorithm.

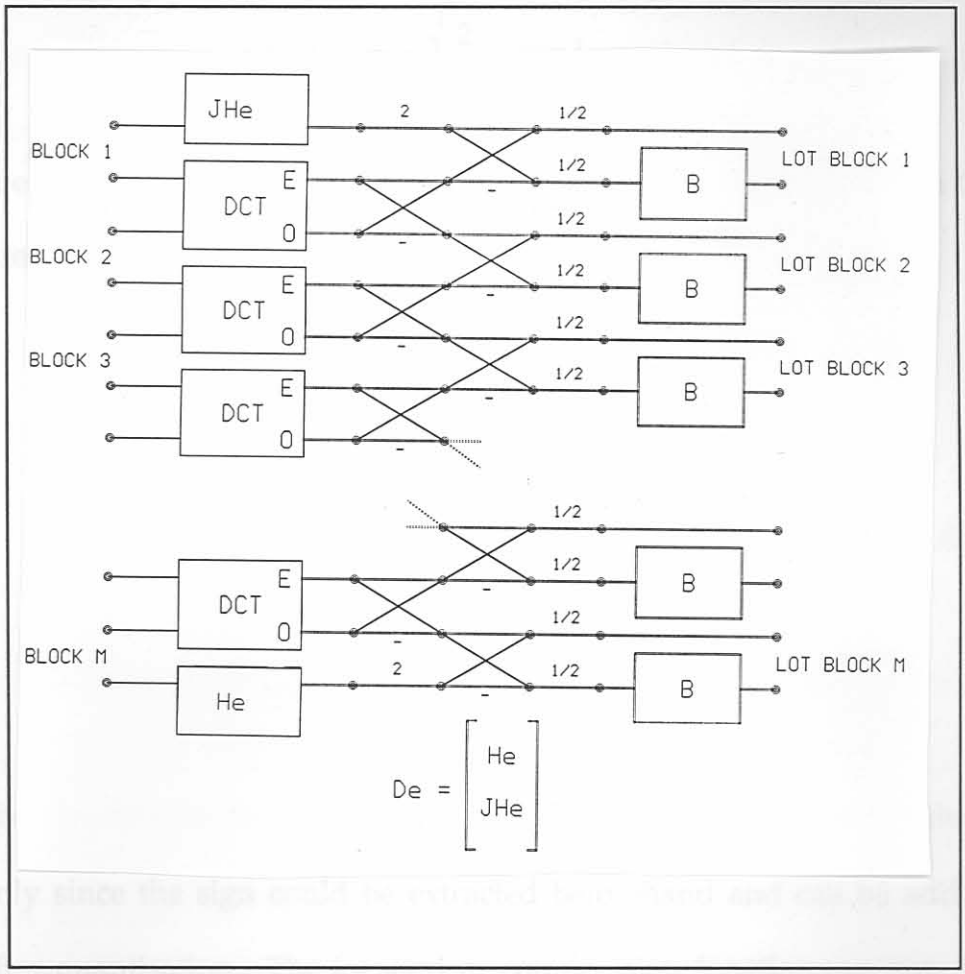

Figure A3 Flowgraph of the fast LOT for a data segment composed of M blocks of size N. Each line consists of N/2 elements. In the figure "E" denotes even and "O" denotes odd.

Appendix B Laplacian Compander

The Laplacian probability density function is given by

$$p(x) = \frac{\alpha}{2}\exp(-\alpha\ |x|) \tag{1}$$

$$where \quad \alpha = \frac{\sqrt{2}}{\sigma}, \quad \sigma^2 = variance$$

The distribution function can be obtained from the density function by integrating from minus infinity to x, i.e.

$$\begin{aligned} F(x) &= \int_{-\infty}^{x} p(x)dx \\ &= \frac{1}{2} + \frac{\alpha}{2}\int_{0}^{x}\exp(-\alpha\ x)dx \\ &= \frac{1}{2} + \left(\frac{-\exp(-\alpha\ x)}{2}\right)\Bigg|_{0}^{x} \\ &= \frac{1}{2}\left[2-\exp(-\alpha\ x)\right], \quad for \quad x \geq 0. \end{aligned} \tag{2}$$

The distribution function has been computed for the positive values only since the sign could be extracted beforehand and can be added after quantisation. The forward or compression function can now be computed by using (Eq.47 pp.47). The output is scaled to be uniformly distributed between plus and minus one half. The companding function is given by

$$g(x) = (y_{max} - y_{min})F[x] + y_{min}$$
$$= 1\left(\frac{1}{2}(2 - \exp(-\alpha\ x))\right) + \frac{1}{2} \qquad (3)$$
$$= \frac{1}{2}(1 - \exp(-\alpha\ x)) \quad for \quad x \geq 0$$

The inverse or expanding function can now be computed by solving for x in (3), i.e.

$$h(g(x)) = -\frac{1}{\alpha}\ln(1 - 2\,g(x)) \quad for \quad g(x) \geq 0 \qquad (4)$$

$g(x)$ is uniformly quantised according to the number of number of bits assigned to the coefficient. If the number of bits is b, the number of levels is 2^b and the compander can be implemented by

$$\hat{x} = h(\,Trunc(g(x)2^b + 2^{-2b})\,) \qquad (5)$$

where the 2^{-2b} is added to obtain the optimum reconstruction levels for the uniformly distributed variable. That is, the Lloyd Max quantiser is applied to the uniformly distributed variable, from which it follows that the optimum reconstruction level is halfway between the two decision levels.

Appendix C Source Coding Quantiser Stepsize

In order to achieve the desired bit rate by using source coding the source have to be quantised. The optimal quantiser for the Laplacian distribution is an uniform quantiser Berger [53]. The problem is to find the stepsize for the uniform quantiser that would achieve this rate. The entropy of a continuously distributed source is given by

$$H(x) = -\sum_{i=0}^{N-1} p_i \log_2 p_i$$

$$\text{where} \quad p_i = \int_{x_i}^{x_{i+1}} p(x)\,dx \qquad (1)$$

$$\text{and} \quad p(x) = \frac{\alpha}{2} e^{-\alpha |x|}$$

For the Laplacian distribution the stepsize can be computed numerically by increasing or decreasing the number of levels N, in (1). However, this would be computationally intensive for large N. For the simulation in this thesis (1) was solved numerically and the results saved in a file. The file was loaded into a lookup table during system initialisation so that no stepsize computation was necessary during coding simulations.

An approximate solution to the stepsize was given by Eggerton [56] and is derived as follows: Since most common probability density functions is monotonously decreasing from zero (for zero average values), there exists a value $\alpha \in [x_i..x_{i+1}]$ for which

$$\int_{x_i}^{x_{i+1}} p(x)\,dx = p(\alpha)\,\Delta \qquad (2)$$

Equation (1) can now be written in terms of (2) as

$$\begin{aligned} H(x) &= -\sum_i \Delta\, p(\alpha_i) \log_2 (\Delta\, p(\alpha_i)) \\ &= -\sum_i \Delta\, p(\alpha_i) \log_2 p(\alpha_i) - \log_2 \Delta \end{aligned} \tag{3}$$

The first term on the right is now intuitively approximated by the entropy of continuous data $H_c(x)$ and a constant ß times the step size

$$\begin{aligned} -\sum_i p(\alpha_i) \log_2 p(\alpha_i)\, \Delta &\approx H(x) + \beta\, \Delta \\ \textit{where} \quad H(x) &= -\int_{-\infty}^{\infty} p(x) \log_2 p(x)\, dx \end{aligned} \tag{4}$$

The value of ß was determined as the one that provides a least squares fit to approximation to

$$H(x) \approx H_c(x) + \beta\, \Delta - \log_2 \Delta \tag{5}$$

and is given by

$$\beta = \frac{\boldsymbol{D}^T \cdot \boldsymbol{Y}}{\boldsymbol{D}^T \cdot \boldsymbol{D}} \tag{6}$$

where

$$\boldsymbol{Y} = \begin{bmatrix} Y(\Delta_1) \\ \vdots \\ Y(\Delta_N) \end{bmatrix} \quad \textit{and} \quad \boldsymbol{D} = \begin{bmatrix} \Delta_1 \\ \vdots \\ \Delta_N \end{bmatrix} \tag{7}$$

Computer simulations were done by Eggerton [56] in which he found that ß was essentially equal to a constant that depended on the distribution and variance of the density function. He determined ß as a function of the deviation σ as follows

Gaussian	$ß=0.082/\sigma$
Laplacian	$ß=0.096/\sigma$
Cauchy	$ß=0.060/\sigma$

With these values of ß the step sizes of the uniform quantiser can be easily computed.

Appendix D Rate Distortion Simulation Parameters

The first order Markov model was used as model for the class of images for which the rate distortion simulation was done. This model was chosen for the lack of a large enough database of images that would be representative of the images the encoder could encounter. The model as defined previously is given by

$$R(x) = \sigma^2 e^{-\alpha |x|} = \sigma^2 \rho^{|x|}$$
$$\textit{where} \quad \rho = e^{-\alpha} \quad \textit{or} \quad \alpha = -\ln \rho \,, \qquad (1)$$
$$\textit{and} \quad \sigma^2 \quad \textit{is the image variance.}$$

The power spectral density can be computed by taking the Fourier transform of the correlation function -

$$S(\omega) = \int_{-\infty}^{\infty} R(x)\, e^{-j\omega x}\, dx \qquad (2)$$

By taking advantage of the odd/even symmetries of the cosine and sine functions, as well as the symmetry of the correlation function, (2) can be written as

$$S(\omega) = 2 \int_{0}^{\infty} R(x) \cos\omega x \; dx \qquad (3)$$

The power spectral density can easily be computed by replacing (1) in (3), i.e.

$$\begin{aligned} S(\omega) &= 2\sigma^2 \int_0^\infty e^{-\alpha x} \cos \omega x \, dx \\ &= 2\sigma^2 \left[\frac{e^{-\alpha x}\left(\cos \omega x + \omega \sin \omega x\right)}{\alpha^2 + \omega^2} \right] \Bigg|_0^\infty \\ &= 2\sigma^2 \left(0 - \frac{1(-\alpha + 0)}{\alpha^2 + \omega^2} \right) \\ &= 2\sigma^2 \frac{\alpha}{\alpha^2 + \omega^2} \end{aligned} \tag{4}$$

For a discrete system the radial frequency can be written in terms of an index

$$\omega = \frac{2\pi}{N} x \qquad x = 0,1,2,\ldots,\frac{N}{2}-1. \tag{5}$$

where N is the image dimension. The frequency weighing function of the human visual system as derived by Mannos and Sakrison [16] is

of the form

$$A(f_r) \approx 2.6\left(0.0192 + 0.114 f_r\right) e^{-(0.114 f_r)^{1.1}} \tag{6}$$

The nonlinear function g is of the form

$$g(u) = u^{0.33} \tag{7}$$

To do the rate distortion simulation the threshold μ has to be calculated for the desired rate R to satisfy

$$R(\mu) = \pi \int_{S_{HVS}(f_r) > \mu} \log_2 \left[\frac{S_{HVS}(f_r)}{\mu} \right] f_r \, df_r \tag{8}$$

where the power spectral density of the human visual system (HVS) is the

weighted power spectral density of the Markov model given by (4), i.e.

$$S_{HVS}(f_r) = \left|A(f_r)\right|^2 S(f_r) \tag{9}$$

To implement the HVS, it has been shown that for the given image the maximum visual frequency is equal to 6.18 cycles/degree (Table I). The radial frequency f_r can be written in terms of the discrete grid as follows

$$f_r = 6.18\sqrt{(x/N)^2+(y/N)^2} \qquad x,y = 0,1,2,\ldots,N-1 \tag{10}$$

References

Books:

[1] William K. Pratt, **"Digital Image Processing"**, *John Wiley & Sons*, 1978.

[2] Arun N. Netravali, Barry G. Haskell, **"Digital Pictures: Representation and Compression"**, *Plenum Press*, 1988.

[3] Andrew J. Viterbi, Jim K. Omura, **"Principles of Digital Communication and Coding"**, *McGraw-Hill*, 1979.

Image Coding: General:

[4] A.K.Jain, **"Image Data Compression: A Review"**, *Proc. IEEE*, VOL.69, NO.3, pp.349-383, March 1981.

[5] W.H.Chen and C.H.Smith, **"Adaptive Coding of Monochrome and Color Images"**, *IEEE Trans. Commun.*, VOL.COM-25, NO.11, pp.1285-1292, November 1977.

[6] A.Habibi, **"Survey of Adaptive Image Coding Techniques"**, *IEEE Tran. Commun.*, VOL.COM-25, NO.11, pp.1275-1284, November 1977.

[7] A.N.Netravali and J.O.Limb, **"Picture Coding: A Review"**, *Proc. IEEE*, VOL.68, NO.3, pp.366-406, pp. , March 1980.

[8] K.N.Ngan, K.S.Leong and H. Singh, **"A HVS-weighted cosine transform coding scheme with adaptive quantisation"**, *SPIE*, VOL.1001 Visual Communications and Image Processing 1988.

[9] R.Forchheimer and T.Kronander, **"Image Coding- From Waveforms to Animation"**, *IEEE Trans. Acoust., Speech, Signal Processing*, VOL.37, NO.12, pp.2008-2023, December 1989.

[10] P.Camana, **"Video-bandwidth compression a study in tradeoffs"**, *IEEE Spectrum*, pp.24-29, June 1979.

[11] H.S.Malvar and D.H.Staelin, **"Optimal Pre- and Postfilters for Multichannel Signal Processing"**, *IEEE Trans. Acoust., Speech, Signal Processing*, VOL.ASSP-36, NO.2, pp.287-289, February 1988.

[12] W.J.Zhang,S.Y. Yu and H.B.Chen, **"A New Adaptive Classified Transform**

Coding Method", *IEEE ICASSP* 1989, pp.1835-1837.

[13] J.A.Roese, W.K.Pratt and G.S.Robinson, **"Interframe Cosine Transform Image Coding"**, *IEEE Trans. Commun.*, VOL.COM-25, NO.11, pp.1329-1338, November 1977.

[14] J.W.Woods and S.D.O'Neal, **"Subband Coding of Images"**, *IEEE Trans. Acoust., Speech, Signal Processing*, VOL.ASSP-34, NO.5, pp.1278-1288, October 1986.

[15] L.Wang and M.Goldberg, **"Progressive Image Transmission by Transform Coefficient Residal Error Quantisation"**, *IEEE Trans. Commun.*, VOL.COM-36, NO.1, pp.75-87, January 1988.

Rate Distortion Theory & Visual Fidelity Criterion:

[16] J.L.Mannos and D.J.Sakrison, **"The Effects of a Visual Fidelity Criterion on the Encoding of Images"**, *IEEE Trans. Infrom. Theory*, VOL.IT-20, NO.4, pp.525-536, July 1974.

[17] H.Lothscheller, **"A Subjectively Adapted Image Communication System"**, *IEEE Tran. Commun.*, VOL.COM-32, NO.12, pp.1316-1322, December 1984.

[18] L.D.Davisson, **"Rate-Distortion Theory and Application"**, *Proc. IEEE*, VOL.60, NO.7, pp.800-807, July 1972.

[19] D.J.Sakrison and V.R.Algazi, **"Comparison of Line-by-Line and Two-Dimensional Encoding of Random Images"**, *IEEE Tran. Inform. Theory*, VOL.IT-17, NO.4, pp.386-398, July 1971.

[20] D.J.Sakrison, **"The Rate of a Class of Random Processes"**, *IEEE Tran. Inform. Theory*, VOL.IT-16, NO.1, pp.10-16, January 1970.

[21] D.L.Neuhoff, R.M.Gray and L.D.Davisson, **"Fixed Rate Universal Block Source Coding with a FIdelity Criterion"**, *IEEE Trans. Inform. Theory*, VOL.IT-21, NO.5, pp.511-523, September 1975.

[22] F.X.J.Lukas and Z.L.Budrikis, **"Picture Quality Prediction Based on a Visual Model"**, *IEEE Trans. Commun.*, VOL.COM-30, NO.7, pp.1679-1692, July 1982.

[23] Z.L.Budrikis, **"Visual Fidelity Criterion and Modeling"**, *Proc. IEEE*, VOL.60, NO.7, pp.771-779, July 1972.

[24] J.Ziv, **"Coding of Sources With Unknown Statitics-Part I: Probability of**

Encoding Error", *IEEE Trans. Inform. Theory*, VOL.IT-18, NO.3, pp.384-394, May 1972.

[25] J.Ziv, **"Coding of Sources With Unknown Statistics- Part II: Distortion Relative to a Fidelity Criterion"**, *IEEE Trans. Inform. Theory*, VOL.IT-18, NO.3, pp.389-394, May 1972.

[26] M.I. Lu and C.F.Chen, **"An Encoding Procedure and a Decoding Procedure for a New Modified Huffman Code"**, *IEEE Trans. Acoust., Speech, Signal Processing*, VOL.ASSP-38, NO.1, pp.128-136, January 1990.

[27] W.Frei and B.Baxter, **"Rate-Distortion Coding Simulation for Color Images"**, *IEEE Trans. Commun.*, VOL.COM-25, NO.11, pp.1385-1392, November 1977.

Transforms & Filters:

[28] A.K.Jain, **"A Fast Karhunen-Loeve Transform for a Class of Random Processes"**, *IEEE Trans. Commun.*, pp.1023-1029, September 1976.

[29] J.B.Burl, **"Estimating the Basis Functions of the Karhunen Loève Transform"**, *IEEE Trans. Acoust., Speech, Signal Processing*, VOL.ASSP-37, NO.1, pp.99-105, January 1989.

[30] R.C.Reininger and J.D.Gibson, **"Distribution of the Two-Dimensional DCT Coefficients for images"**, *IEEE Tran. Commun.*, VOL.COM-31, pp.835-839, NO.6, June 1983.

[31] N.Ahmed ,T.Natarjan and K.R.Rao, **"Discrete Cosine Transform"**, *IEEE Trans. Comput.(Corresp.)*, VOL.C-23, pp.90-93, January 1974.

[32] N.R.Murthy and M.N.S.Swamy, **"On the Algorithms for the Computation of Even Discrete Cosine Transform-2 (EDCT-2) of Real Sequences"**, *IEEE Trans. Circuits and Systems*, VOL.37, NO.5, pp.625-627, May 1990.

[33] Z.Wang, **"Reconsideration of "A Fast Computational Algorithm for the Discrete Cosine Transform"**, *IEEE Trans. Commun.*, VOL.COM-31, NO.1, pp.121-123, January 1983.

[34] F.A.Kamangar and K.R.Rao, **"Fast Algorithms for the 2-D Discrete Cosine Transform"**, *IEEE Trans. Comput.*, VOL.C-31, NO.9, pp.899-906, September 1982.

[35] W.Chen, C.Harrison and S.C.Fralick, **"A Fast Computational Algorithm for the Discrete Cosine Transform"**, *IEEE Trans. Commun.*, VOL.COM-25, NO.9, pp.1004-1009, September 1977.

[36] M.Hamidi and J.Pearl, **"Comparison of the Cosine and Fourier Transforms of Markov-1 Signals"**, *IEEE Trans. Acoust., Speech, Signal Processing*, pp. 428-429, October 1976.

[37] Z.Wang, **"Fast Algorithms for the Discrete W Transform and for the Discrete Fourier Transform"**, *IEEE Trans. Acoust., Speech, Signal Processing*, VOL.ASSP-32, NO.4, pp-803-816, August 1984.

[38] P.P.Vaidyanathan and S.K.Mitra, **"Polyphase Networks, Block Digital Filtering, LPTV Systems, and Alias-Free QMF Banks: A Unified Approach Based on Pseudocirculants"**, *IEEE Trans. Acoust., Speech, Signal Processing*, VOL.ASSP-36, NO.3, pp.381-391, March 1988.

[39] M.D.Flickner and N.Ahmed, **"A Derivation for the Discrete Cosine Transform"**, Proc. IEEE, VOL.70, NO.9, pp.1132-1134, September 1982.

[40] K.Sivaraman and K.P.Rajappan, **"A Study of Rectangular Transforms for Data Compression"**, *IEEE Trans. Acoust., Speech, Signal Processing*, VOL.ASSP-32, NO.4, August 1984.

[41] W.Kou and J.W.Mark, **"A New Look at DCT-Type Transforms"**, *IEEE Trans. Acoust., Speech, Signal Processing*, VOL.ASSP-37, NO.12, pp. 1899-1908, December 1989.

[42] P.P.Vaidynathan, T.Q.Nguyen, Z.Doganata and T.Saramäki, **"Improved Technique for DEsign of Perfect Reconstruction FIR QMF Banks with Lossless Polyphase Matrices"**, *IEEE Trans. Acoust., Speech, Signal Processing*, VOL.ASSP-37, NO.7, pp.1042-1056, July 1989.

[43] A.N.Akansu and R.A.Haddad, **"On Asymmetrical Performance of Discrete Cosine Transforms"**, *IEEE Trans. Acoust., Speech, Signal Processing*, VOL.ASSP-38, NO.1, pp154-156, January 1990.

[44] B.G.Lee, **"Input and Output Index Mappings for a Prime-Factor-Decomposed Computation of Discrete Cosine Transform"**, *IEEE trans. Acoust., Speech, Signal Processing*, VOL.ASSP-37, NO.2, pp.237-244, February 1989.

[45] A.K.Jain, **"A Sinusoidal Family of Unitary Transforms"**, *IEEE Trans. Pattern Analysis and Machine Intelligence*, VOL.PAMI-1, NO.4, pp.356-365, October 1979.

[46] M.Vetterli and D.Le Gall, **"Perfect Reconstruction FIR Filter Banks: Some Properties and Factorizations"**, *IEEE Trans. Acoust., Speech, Signal Processing*, VOL.ASSP-37, NO.7, pp.1057-1071. July 1989.

[47] J.Kovacevic, D.J.Le Gall, M.Verrerli, **"Image Coding with Windowed Modulated Filter Banks"**, *IEEE ICASSP* 1989, pp.1949-1951.

Image Modelling:

[48] J.W.Woods, **"Two-Dimensional Discrete Markovian Fields"**, *IEEE Tran. Inform. Theory*, VOL.IT-18, NO.2, pp.232-240, March 1972.

[49] R.L.Kashyap, **"Univariate and Multivariate Random Field Models for Images"**, *Computer Graphics and Image Processing 12*, 257-270, 1980.

[50] A.Dembo, **"The Relation Between Maximum Likelihood Estimation of Structured Covariance Matrices and Periodograms"**, *IEEE Trans. Acoust., Speech, Signal Processing*, VOL.ASSP-34, NO.6, pp.1661-1662, December 1986.

[51] A.K.Jain, **"Advances in Mathematical Models for Image Processing"**, *Proc. IEEE*, VOL.69, NO.5, pp.122-148, May 1981.

Quantisation:

[52] A.Segall, **"Bit Allocation and Encoding for Vector Sources"**, *IEEE Tran. Inform. Theory.*, VOL.IT-22, NO.2, pp.162-169, March 1976.

[53] T.Berger, **"Optimum Quantisers and Permutation Codes"**, *IEEE Tran Inform. Theory*, VOL.IT-18, NO.6, pp.759-765, November 1972.

[54] D.K.Sharma, **"Design of Absolutely Optimal Quantizers for a Wide Class of Distortion Measures"**, *IEEE Trans. Inform. Theory*, VOL.IT-24, NO.6, pp.693-702, November 1978.

[55] A.N.Netravali and R.Saigal, **"Optimum Quantiser Design Using a Fixed-Point Algorithm"**, *The Bell System Technical Journal*, VOL.55, NO.9, pp.1423-1435, November 1976.

[56] J.D.Eggerton and M.D.Srinath, **"A Visually Weighted Quantisation Scheme**

for Image Bandwidth Compression at Low Data Rates", *IEEE tran. Commun.*, VOL.COM-34, NO.8, pp.840-847, August 1986.

[57] P.Kabal, **"Quantisers for the Gamma Distribution and Other Symmetrical Distributions"**, *IEEE Trans. Acoust., Speech, Signal Processing*, VOL.ASSP-32, NO.4, pp.836-841, August 1984.

[58] K.Tzou, **"A Fast Computational Approach to the Design of Block Quantization"**, *IEEE Trans. Acoust., Speech, Signal Processing*, VOL.ASSP-35, NO.2, pp.235-237, February 1987.

[59] R.C.Wood, **"On Optimum Quantisation"**, *IEEE Trans. Inform. Theory*, VOL.IT-15, NO.2, pp.248-252, March 1969.

[60] J.B.O'Neal (JR.), **"Differential Pulse-Code Modulation (PCM) with Entropy Coding"**, *IEEE Trans. Inform. Theory*, VOL.IT-22, NO.2, pp.169-174, March 1976.

LOT based image coding:

[61] P.M.Cassereau, D.H.Staelin and G.de Jager, **"Encoding of Images on a Lapped Orthogonal Transform"**, *IEEE Trans. Commun.*, VOL.COM-37, NO.2, pp.189-193, February 1989.

[62] H.S.Malvar and D.H.Staelin, **"The LOT: Transform Coding Without Blocking Effects"**, *IEEE Trans. Acoust., Speech, Signal Processing*, VOL.ASSP-37, NO.4, pp.553-559, April 1989.

[63] H.S.Malvar, **"Lapped Transforms for Efficient Transform/Subband Coding"**, *IEEE Trans. Acoust., Speech, Signal Processing*, VOL.ASSP-38, NO.6, pp.969-978, June 1990.

[64] D.R.Farrier and D.J.Jeffries, **"Resolution of Signal Wavefronts by Eigenvector Rotation"**, *IEEE Trans. Acoust., Speech, Signal Processing*, VOL.ASSP-35, NO.4,pp564-566, April 1987.

[65] P.Haskell, K.H.Tzou, T.R.Hsing, **"A Lapped-Orthogonal-Transform Based Variable Bit Rate Video Coder for Packet Networks"**, *IEEE ICASSP* 1989, pp.1905-1908.

[66] 'ICASSP 89 Glasgow Scotland'

.....